2019

3D Scaffolds of Polycaprolactone/Copper-Doped Bioactive Glass: Architecture Engineering with Additive Manufacturing and CellularAssessments in a Coculture of Bone Marrow Stem Cells and Endothelial Cells

Xiaoju Wang
Abo Akademi University

Binbin Zhang
University of Wollongong, binbinz@uow.edu.au

Sanna Pitkanen
Tampere University

Miina Ojansivu
Tampere University

Chunlin Xu
Abo Akademi University

Publication Details

Wang, X., Molino, B. Zhang., Pitkanen, S., Ojansivu, M., Xu, C., Hannula, M., Hyttinen, J., Miettinen, S., Hupa, L. & Wallace, G. (2019). 3D Scaffolds of Polycaprolactone/Copper-Doped Bioactive Glass: Architecture Engineering with Additive Manufacturing and CellularAssessments in a Coculture of Bone Marrow Stem Cells and Endothelial Cells. ACS Biomaterials Science and Engineering, 5 (9), 4496-4510.

See next page for additional authors

3D Scaffolds of Polycaprolactone/Copper-Doped Bioactive Glass: Architecture Engineering with Additive Manufacturing and CellularAssessments in a Coculture of Bone Marrow Stem Cells and Endothelial Cells

Abstract
The local delivery of Cu2+ from copper-doped bioactive glass (Cu-BaG) was combined with 3D printing of polycaprolactone (PCL) scaffolds for its potent angiogenic effect in bone tissue engineering. PCL and Cu-BaG were, respectively, dissolved and dispersed in acetone to formulate a moderately homogeneous ink. The PCL/Cu-BaG scaffolds were fabricated via direct ink writing into a cold ethanol bath. The architecture of the printed scaffolds, including strut diameter, strut spacing, and porosity, were investigated and characterized. The PCL/Cu-BaG scaffolds showed a Cu-BaG content-dependent mechanical property, as the compressive Young's modulus ranged from 7 to 13 MPa at an apparent porosity of 60%. The ion dissolution behavior in simulated body fluid was evaluated, and the hydroxyapatite-like precipitation on the strut surface was confirmed. Furthermore, the cytocompatibility of the PCL/Cu-BaG scaffolds was assessed in human bone marrow stem cell (hBMSC) culture, and a dose-dependent cytotoxicity of Cu2+ was observed. Here, the PCL/BaG scaffold induced the higher expression of late osteogenic genes OSTEOCALCIN and DLX5 in comparison to the PCL scaffold. The doping of Cu2+ in BaG elicited higher expression of the early osteogenic marker gene RUNX2a but decreased the expression of late osteogenic marker genes OSTEOCALCIN and DLX5 in comparison to the PCL/BaG scaffold, demonstrating the suppressing effect of Cu2+ on osteogenic differentiation of hBMSCs. In a coculture of hBMSCs and human umbilical vein endothelial cells, both the PCL/BaG and PCL/Cu-BaG scaffolds stimulated the formation of a denser tubule network, compared to the PCL scaffold. Meanwhile, only slightly higher gene expression of vWF was observed with the PCL/Cu-BaG scaffold than with the PCL/BaG scaffold, indicating the potent angiogenic effect of the released Cu2+.

Keywords
additive, engineering, bioactive, polycaprolactone/copper-doped, scaffolds, manufacturing, 3d, marrow, cellularassessments, bone, stem, coculture, cells, architecture, glass:, endothelial

Publication Details
Wang, X., Molino, B. Zhang., Pitkanen, S., Ojansivu, M., Xu, C., Hannula, M., Hyttinen, J., Miettinen, S., Hupa, L. & Wallace, G. (2019). 3D Scaffolds of Polycaprolactone/Copper-Doped Bioactive Glass: Architecture Engineering with Additive Manufacturing and CellularAssessments in a Coculture of Bone Marrow Stem Cells and Endothelial Cells. ACS Biomaterials Science and Engineering, 5 (9), 4496-4510.

Authors
Xiaoju Wang, Binbin Zhang, Sanna Pitkanen, Miina Ojansivu, Chunlin Xu, Markus Hannula, Jari A. Hyttinen, Susanna S. Miettinen, Leena Hupa, and Gordon G. Wallace

ACS Biomaterials SCIENCE & ENGINEERING

Article

Cite This: ACS Biomater. Sci. Eng. 2019, 5, 4496−4510

pubs.acs.org/journal/abseba

3D Scaffolds of Polycaprolactone/Copper-Doped Bioactive Glass: Architecture Engineering with Additive Manufacturing and Cellular Assessments in a Coculture of Bone Marrow Stem Cells and Endothelial Cells

Xiaoju Wang,[*,†,#] Binbin Zhang Molino,[‡,#] Sanna Pitkänen,[§,∥,#] Miina Ojansivu,[§,∥] Chunlin Xu,[†] Markus Hannula,[⊥] Jari Hyttinen,[⊥] Susanna Miettinen,[§,∥] Leena Hupa,[†] and Gordon Wallace[‡]

[†]Johan Gadolin Process Chemistry Centre, Åbo Akademi University, Piispankatu 8, 20500 Turku, Finland

[‡]ARC Centre of Excellence for Electromaterials Science, Intelligent Polymer Research Institute, University of Wollongong, Northfields Avenue, Wollongong, New South Wales 2522, Australia

[§]Adult Stem Cell Group, BioMediTech, Faculty of Medicine and Health Technology, Tampere University, Arvo Ylpön katu 34, P.O. BOX 100, FI-33014 Tampere, Finland

[∥]Research, Development and Innovation Centre, Tampere University Hospital, Arvo Ylpön katu 6, P.O. BOX 2000, FI-33521 Tampere, Finland

[⊥]Computational Biophysics and Imaging Group, BioMediTech, Faculty of Medicine and Health Technology, Tampere University, FI-33014 Tampere, Finland

Supporting Information

ABSTRACT: The local delivery of Cu^{2+} from copper-doped bioactive glass (Cu-BaG) was combined with 3D printing of polycaprolactone (PCL) scaffolds for its potent angiogenic effect in bone tissue engineering. PCL and Cu-BaG were, respectively, dissolved and dispersed in acetone to formulate a moderately homogeneous ink. The PCL/Cu-BaG scaffolds were fabricated via direct ink writing into a cold ethanol bath. The architecture of the printed scaffolds, including strut diameter, strut spacing, and porosity, were investigated and characterized. The PCL/Cu-BaG scaffolds showed a Cu-BaG content-dependent mechanical property, as the compressive Young's modulus ranged from 7 to 13 MPa at an apparent porosity of 60%. The ion dissolution behavior in simulated body fluid was evaluated, and the hydroxyapatite-like precipitation on the strut surface was confirmed. Furthermore, the cytocompatibility of the PCL/Cu-BaG scaffolds was assessed in human bone marrow stem cell (hBMSC) culture, and a dose-dependent cytotoxicity of Cu^{2+} was observed. Here, the PCL/BaG scaffold induced the higher expression of late osteogenic genes *OSTEOCALCIN* and *DLX5* in comparison to the PCL scaffold. The doping of Cu^{2+} in BaG elicited higher expression of the early osteogenic marker gene *RUNX2a* but decreased the expression of late osteogenic marker genes *OSTEOCALCIN* and *DLX5* in comparison to the PCL/BaG scaffold, demonstrating the suppressing effect of Cu^{2+} on osteogenic differentiation of hBMSCs. In a coculture of hBMSCs and human umbilical vein endothelial cells, both the PCL/BaG and PCL/Cu-BaG scaffolds stimulated the formation of a denser tubule network, compared to the PCL scaffold. Meanwhile, only slightly higher gene expression of *vWF* was observed with the PCL/Cu-BaG scaffold than with the PCL/BaG scaffold, indicating the potent angiogenic effect of the released Cu^{2+}.

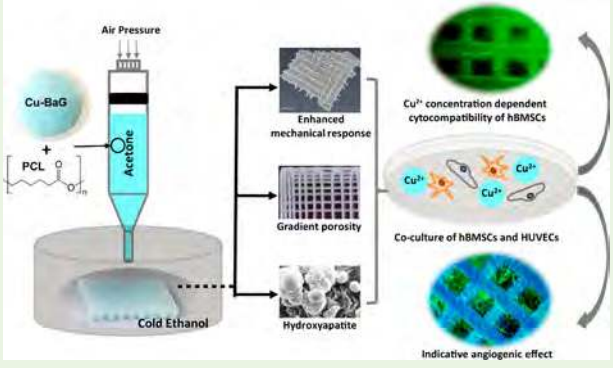

KEYWORDS: *3D printing, tissue engineering scaffold, angiogenesis, polycaprolactone, copper-doped bioactive glass, gradient porosity, coculture of mesenchymal stem cells and endothelial cells*

INTRODUCTION

Synthetic bone grafts that resemble the architecture and composition of the bone extracellular matrix are always sought by biomaterial scientists and surgeons to overcome the limitations of bone autografts and allografts in the treatments of large bone defects in patients.[1−3] The application of tissue engineering (TE) scaffolds has emerged as a strategic approach for bone reconstitution, as it combines the engineered biomaterial structure, soluble/mechanical factors (e.g., release of stimulating bio(macro)molecules/ions), and regenerative cells to provide a structural and physiological support to the spatial tissue growth.[4,5]

Received: January 23, 2019
Accepted: July 18, 2019
Published: July 18, 2019

DOI: 10.1021/acsbiomaterials.9b00105
ACS Biomater. Sci. Eng. 2019, 5, 4496−4510

As the first man-made biomaterial capable of forming chemical bonding to bone,[6] bioactive glasses (BaGs) have been extensively explored during the past several decades in bone TE because of their osteostimulative capability to guide and stimulate the bone growth.[7−9] However, successful neovascularization (the sprouting of blood vessels) in the bone TE constructs remains challenging.[10,11] Several well-established compositions of silicate BaGs, such as 45S5 and S53P4, are capable of inducing angiogenic differentiation of mesenchymal stem cells (MSCs).[12,13] This is attributed to their ionic dissolution products of soluble Ca, Si, and P that can upregulate the genes related to angiogenesis, such as those encoding vascular endothelial growth factor (VEGF) and basic fibroblast growth factor (bFGF).[13,14] Moreover, the essential participation of Cu^{2+} in angiogenesis has been acknowledged: Cu^{2+} in a proper dosage has a clear proangiogenic function by activating a group of proangiogenic growth factors, including VEGF and platelet-derived growth factor (PDGF), therefore promoting endothelial cell proliferation and tubule formation.[15−17] At present, the local delivery of Cu^{2+} from the Cu-doped BaG to induce angiogenesis has been investigated in various forms, e.g., porous scaffold of Cu-doped mesoporous BaG,[18] composite hydrogel containing Cu-doped mesoporous BaG,[19] functional coating of Cu-doped BaG nanoparticles and electrospun nanofibers of Cu-doped BaG.[20−22] Strategically, the incorporation of Cu-doped BaG in bone TE scaffolds may offer a straightforward approach to address the neovascularization challenge in bone tissue regeneration.

The critical aspects to be taken into consideration when designing a bone TE scaffold are the selection of suitable biomaterials to support cell adhesion and proliferation as well as the definitive structural parameters of the scaffold to mimic the native bone tissue. Polycaprolactone (PCL), a bioresorbable polymer extensively used in various biomedical applications, offers excellent material properties and cytocompatibility.[23] The extrusion-based 3D printing (3DP) techniques offer a high-level control of the scaffold architecture, including pore size, distribution, and interconnectivity.[24] Previously, the TE scaffolds for bone regeneration manufactured by the 3DP using PCL or its composites with inorganic minerals such as the microparticles of tricalcium phosphate,[25] hydroxyapatite, and calcium polyphosphate have been studied.[26,27] Conventionally, the melted PCL is used as the carrier phase for the mineral microparticles, and the printed constructs keep the shape fidelity through fast cooling after being extruded through the nozzle in 3DP.

In the current study, a solvent-based approach was proposed to prepare the well-dispersed BaG microparticles of Cu-doped S53P4 (S53P4−Cu1) in PCL solution (in acetone) as a homogeneous ink fed in the direct ink writing (DIW), and the printed struts solidified rapidly in the cold ethanol due to the solubility change of PCL, thus facilitating the fabrication of the PCL/Cu-BaG composite scaffolds. This method offers a facile printing as no heating is needed and also extends the possibility to incorporate other bioactive molecules, such as growth factors, within the scaffold during the printing process. Then, the ion dissolution behavior and bioactivity (in terms of supporting the hydroxyapatite precipitation) of the composite scaffolds were evaluated in simulated body fluid (SBF). Furthermore, the cytocompatibility of the composite scaffolds as well as the impact of the ion release on the early osteogenic differentiation of human bone marrow stem cells (hBMSCs) were evaluated *in vitro*. Finally, we studied whether the Cu^{2+} released from the 3D scaffolds could promote the angiogenesis in a coculture of hBMSCs and human umbilical vein endothelial cells (HUVECs). The observations are indicative for utilizing the Cu-doped BaG aiming at enhancing the vascularization in TE scaffolds.

MATERIALS AND EXPERIMENTAL

Glass Melting of BaGs (S53P4 and S53P4−Cu1) and Preparation of BaG Microparticles. Two BaGs, S53P4 (53% SiO_2−4%P_2O_5−20%CaO−23%Na_2O wt %) and S53P4−Cu1 (53% SiO_2−4%P_2O_5−19%CaO−23%Na_2O−1%CuO wt %), were prepared using the melt-quenching method. The batches consisted of analytical grade reagents Na_2CO_3, $CaCO_3$, $CaHPO_4{\cdot}2H_2O$, $Cu(NO_3)_2{\cdot}2.5H_2O$ (all purchased from Sigma-Aldrich), and Belgian glass quality quartz sand (0.32 mm, Varnia Oy). The batches were melted in a Pt crucible at 1360 °C for 3 h, cast, annealed, crushed, and remelted to ensure the homogeneity. The annealed glass block was crushed and gradually fractionated with a set of woven wire mesh sieves with #mm from 500 μm down to 45 μm (laboratory test sieves, Retsch GmbH) to give several powdered fractions. The finest powder fraction, which could pass through the #mm = 45 μm sieve, was further milled for 10 min using a benchtop planetary ball mill (MinMill, Philips) to obtain the fine particles of BaG for the DIW ink formulation.

Scaffolds Fabrication via DIW. A 30 g portion of PCL (M_w = 80 000, Aldrich) was dissolved in 100 mL of acetone overnight in a 50 °C water bath to obtain a viscous solution, which was then used as the carrier phase for the BaG particles in the ink formulation. The BaG particles were homogeneously dispersed into the viscose PCL solution using a planetary centrifugal mixer (ARE-250, Thinky Corporation) at a rotation speed of 2000 rpm. The compositional ratio between the PCL and BaG was adjusted to 4:1, 2:1, or 1:1, according to the content of PCL and BaG in wt %.

The scaffold fabrication via DIW was carried out using an adapted Korean Institute for Machinery and Materials (KIMM) Bioplotter. The KIMM Bioplotter software was used to produce a G-code tooling path for printing. Square block models (x = 10 mm, y = 10 mm, and z = 1, 2, or 4 mm) were designed with the Bioplotter software, and the strut spacing (SS) was defined as either 400 or 800 μm between the center of the struts. For the scaffolds with a gradient porosity, the SS was decreased from the center to the edge of the scaffold, from 800 to 200 μm. The viscous ink as formulated was loaded into a fluid dispensing system (Optimum by Nordson EFD), with the syringe barrel installed onto the KIMM printer and connected to an air pressure regulator. A precision tip made of stainless steel (25GA, Nordson EFD) was used as the dispensing nozzle. The scaffolds were printed layer-by-layer through extruding the ink into a cold ethanol bath. The feed rate was kept constant at 2 mm s^{-1}, and the extrusion pressure was then manually adjusted in the range 1.5−3.0 bar according to the viscosity of the ink for an optimal printing process. The scaffolds were then soaked in absolute ethanol for 24 h, and the ethanol was replaced every 8 h to complete the phase exchange of PCL from acetone to ethanol. Finally, the scaffolds were collected and dried in air before further characterizations.

Scaffold Imaging with Optical Microscopy, Scanning Electron Microscopy (SEM), and Micro Computed Tomography (μ-CT). The microscopic features of scaffolds were observed by using a LEICA M205A optical microscope. The reported strut diameter and strut spacing were assessed in triplicate (n = 3). The morphological features of the scaffold strut were characterized by using SEM. To assess the macroporosity, μ-CT was used to analyze the inner structure of the scaffolds. The imaging was performed with an Xradia MicroXCT-400 (Zeiss, Pleasanton, CA) device: 1600 projections were taken with a pixel size of 19.70 μm. The source voltage was set to 80 kV, and the source current was 125 μA. To achieve the desired image quality, a 3 s exposure time was used. The device manufacturer's XMReconstructor software was used to reconstruct the 3D volumes. Image segmentation was done with Avizo software (Thermo Fisher Scientific, Waltham, MA) using manual thresholding. Approximately 8.2 × 8.2 × 2.4 mm

DOI: 10.1021/acsbiomaterials.9b00105
ACS Biomater. Sci. Eng. 2019, 5, 4496−4510

volumes were selected, and the porosity, strut size, and pore size of the 3D scaffolds were calculated with the BoneJ plugin in the Fiji program.

Thermogravimetric (TG) Analysis. TG analysis of the scaffolds was performed using a differential thermal analysis instrument (Netzsch STA 449F1) in the gas flow of synthetic air at a speed of 100 mL min^{-1}. The temperature ramped up to 850 °C at an elevating rate of 10 °C min^{-1}. The BaG wt % of the scaffold was determined as relative to the residue content in the TG analysis.

Mechanical Tests. The compressive response of the printed scaffolds was measured with a Shimadzu EZ-L Universal Mechanical Tester. Scaffolds were compressed at 1 mm min^{-1} and a maximum loading of 500 N was applied. When calculating the strength, the dimensions along the *x*, *y*, and *z*-axes measured with a digital caliper were used. Strain was registered as a function of stress for an applied and increasing force and the measurements were conducted in triplicate to elaborate the compressive modulus based on the stress vs strain curves.

Ion Release Study of PCL/Cu-BaG Scaffolds in SBF. The SBF was prepared according to the protocol of Kokubo, and the exact composition is presented in the Supporting Information S1.[28] The 3D scaffolds were immersed in 10 mL of SBF in airtight polyethylene containers that were placed in an incubating orbital shaker held at 37 °C and agitated at 100 rpm. The samples were incubated for a total period of 30 days and sampled at intervals of 6 h, 24 h, 3 days (3 d), 7 d, 14 d, 22 d, and 30 d. At each time point, 0.5 mL of the immersion solution was sampled, and 0.5 mL of fresh SBF was additionally replenished for a continued immersion. The ionic concentrations of Ca, P, Si, and Cu ions in the sampled solution were analyzed with an inductively coupled plasma optical emission spectrometer (ICP-OES) (Optima 5300 DV, PerkinElmer, Shelton, CT). For the ICP-OES measurements, the sampled aliquots were diluted 10 times with deionized H_2O. At the end of the immersion test, the scaffolds were carefully collected, washed extensively with ethanol, and dried in the air. The surface morphology and elemental analysis of the scaffolds were characterized with an SEM-EDXA instrument (EDXA, LEO Gemini 1530 with a Thermo Scientific UltraDry Silicon Drift Detector, X-ray detector by Thermo Scientific).

Isolation and Characterization of hBMSCs and HUVECs. The hBMSCs were isolated from a bone marrow aspirate sample obtained from a surgical procedure at the Department of Orthopedics and Traumatology, Tampere University Hospital, with the patient's consent. The hBMSCs used in the study were harvested from a female donor of 80 years of age. The study was conducted in accordance with the Ethics Committee of the Pirkanmaa Hospital District, Tampere (R15174). hBMSCs were isolated using centrifugation through a Ficoll gradient. First, the bone marrow aspirate was suspended in Dulbecco's phosphate buffered saline (DPBS), and the solution was pushed through a 100 μm cell strainer. The bone marrow aspirate solution was centrifuged, and the fat layer was removed. Thereafter, the bone marrow aspirate solution was pipetted carefully on top of a Ficoll gradient (Histopaque-1077; 1.077 g mL^{-1}; Sigma-Aldrich; St. Louis, MO). A 2.6 mL portion of Ficoll (Histopaque; Sigma-Aldrich) per 1 mL of bone marrow aspirate sample was used. The bone marrow aspirate solution was centrifuged for 20 min at 800*g*, and the mononucleated hBMSCs were harvested from an interphase between the Ficoll and plasma phases. The cells were washed twice with 5 mL of MEM Alpha medium (Thermo Fisher Scientific, Waltham, MA) per 1 mL of collected interphase, and the suspension was centrifuged for 15 min at 400*g*. The cell pellet was suspended in basic medium (BM) consisting of MEM Alpha medium (Thermo Fisher Scientific), 5% human serum (HS; BioWest, Nuaillé, France), and 1% antibiotics (100 U mL^{-1} penicillin; 100 U mL^{-1} streptomycin; Lonza, Basel, Switzerland) with 5 ng mL^{-1} human FGF-2 (Miltenyi Biotec; Bergisch Gladbach, Germany). Isolated hBMSCs were expanded in BM at 37 °C in 5% CO_2, and medium was changed twice per week. Cells were detached with TrypLE Select (Thermo Fisher Scientific). The experiments were carried out at passage 3.

HUVECs were extracted from the umbilical cord acquired from scheduled Cesarean section at the Department of Obstetrics and Gynecology, Tampere University Hospital, with the donor's consent according to Hamilton et al.[29] The study was conducted in accordance with the Ethics Committee of the Pirkanmaa Hospital District, Tampere (R13019). Briefly, the cord was separated from the placenta; the umbilical vein was cannulated with a 20G needle, and the needle was secured by clamping the cord over the needle with a clamp. The vein was perfused with PBS to wash out blood, and then, the opposing end of the umbilical vein was clamped. Subsequently, the vein was infused with collagenase II (Sigma). The umbilical cord was incubated in a water bath at 37 °C for 15 min. After incubation, the collagenase solution containing HUVECs was flushed from the cord into a 50 mL polypropylene tube. The cells were centrifuged at 1200 rpm for 6 min and resuspended in EGM-2 BulletKit (Lonza) medium supplemented with 2% HS and seeded into 25 cm^3 flasks. The HUVECs were cultured at 37 °C in 5% CO_2, and the medium was changed twice per week. Cells were detached with TrypLE Select (Thermo Fisher Scientific). The experiments were carried out at passage 3.

To verify the mesenchymal origin of the hBMSCs and the endothelial phenotype of HUVECs, surface marker expression was characterized by flow cytometry (FACSAria; BD Biosciences, Erembodegem, Belgium) as described previously, as documented in Supporting Information S2.[30]

Cell Seeding and Culture on Scaffolds. In the cell culture study, the PCL scaffolds were used as a control to the composite scaffolds; the scaffolds PCL/S53P4 were also included as a Cu-free control to the scaffolds of PCL/S53P4−Cu1. All the tested scaffolds (10 mm × 10 mm × 1 mm) were sterilized by incubating the scaffolds 2 × 10 min in 70% ethanol, and then, the scaffolds were left to dry for 2 h in a biosafety cabinet. Thereafter, the scaffolds were incubated in BM for 48 h prior to cell seeding.

All scaffolds' ability to support hBMSC viability, proliferation, and early osteogenic differentiation was evaluated in hBMSC culture. hBMSCs were seeded, 50 000 per scaffold, in a 50 μL OM (BM with 200 μM ascorbic acid 2-phosphate (Sigma-Aldrich), 10 mM β-glycerophosphate (Sigma-Aldrich), and 5 nM dexamethasone (Sigma-Aldrich)) drop on to the scaffolds. Cells were allowed to attach for 3 h before adding 2 mL of OM per well. The medium was changed to a fresh one twice per week during the experiment.

The scaffolds' ability to support vascularization was assessed in the coculture experiment with hBMSCs and HUVECs. Only PCL, PCL/S53P4 = 4:1, and PCL/S53P4−Cu1 = 4:1 scaffolds were used in the coculture experiment due to the observed cytotoxicity of higher S53P4−Cu1 content with the other compositional ratios. The originally printed scaffolds (10 mm × 10 mm × 1 mm and d = 400 μm) were cut into four quarters for further use. hBMSCs were seeded, 20 000 per scaffold, and cultured for 6 d before seeding an equal amount of HUVECs. After seeding the HUVECs, the medium was changed to EGM-2 (Lonza, Basel, Switzerland). hBMSCs alone were used as a control group and cultured in OM throughout the experiment.

Cell Viability and Proliferation. Cell viability was evaluated qualitatively by staining the hBMSCs with fluorescent live/dead-staining probes (Thermo Fisher Scientific) after 1 d and 14 d of culture. The samples were incubated for 45 min at room temperature in a mixture of 0.5 μM calcein-AM and 0.25 μM ethidium homodimer-1. Images of viable cells (green fluorescence) and dead cells (red fluorescence) were taken using an Olympus IX51 phase contrast microscope with fluorescence optics and Olympus DP30BW camera (Olympus, Tokyo, Japan).

Cell viability was quantitatively analyzed by a lactate dehydrogenase (LDH) activity assay (Abcam, Cambridge, UK). The LDH reduces NAD to NADH, which then interacts with a specific probe to produce a color. The medium samples were collected at every medium change and stored at −20 °C until analysis. The analysis was conducted according to the manufacturer's protocol. After 30 min of incubation at room temperature, the absorbance, i.e., the intensity of the color, was determined at 450 nm with a microplate reader (Victor 1420 Multilabel Counter; Wallac; Turku, Finland).

Cell number was determined quantitatively after 7 d and 14 d of hBMSC culture by analyzing the total amount of DNA by a CyQUANT cell proliferation assay kit (Thermo Fisher Scientific) as reported previously.[31] CyQUANT GR dye emits fluorescence when bound to nucleic acids. Samples were analyzed after two freeze−thaw cycles, and

DOI: 10.1021/acsbiomaterials.9b00105
ACS Biomater. Sci. Eng. 2019, 5, 4496−4510

Table 1. Primer Sequences and Accession Numbers of Genes Analyzed by qRT-PCR

name		5′-sequences-3′	product size (bp)	accession number
hRPLP0	Frw	AATCTCCAGGGGCACCATT	70	NM_001002
	Rev	CGCTGGCTCCCACTTTGT	70	NM_001002
hOSTEOCALCIN	Frw	AGCAAAGGTGCAGCCTTTGT	63	NM_000711
	Rev	GCGCCTGGGTCTCTTCACT	63	NM_000711
hRUNX2a	Frw	CTTCATTCGCCTCACAAACAAC	62	NM_001024630.3
	Rev	TCCTCCTGGAGAAAGTTTGCA	62	NM_001024630.3
hDLX5	Frw	ACCATCCGTCTCAGGAATCG	75	NM_005221.5
	Rev	CCCCCGTAGGGCTGTAGTAGT	75	NM_005221.5

fluorescence was measured at 480/520 nm with a microplate reader (Victor 1420, Wallac).

Cu^{2+} Concentration in Culture Medium of hBMSCs. In the culture of hBMSCs, the medium samples were collected from 3 parallel wells at 2 d, 6 d, and 13 d while the medium was changed and pooled as one sample per time point. The concentration of Cu^{2+} in the sample was analyzed by the ICP-OES analysis using the same protocol as described in the earlier Ion Release Study of PCL/Cu-BaG Scaffolds in SBF section.

Alkaline Phosphatase Activity. Alkaline phosphatase (ALP) activity was determined after 7 d and 14 d of hBMSC culture as described previously.[31] The ALP activity was determined from the same cell lysates as the total DNA content. Absorbance was measured at 405 nm (Victor 1420, Wallac).

Quantitative Real-Time PCR. The relative expression of endothelial marker genes *PECAM* and *vWF* was evaluated with quantitative real-time reverse transcription polymerase chain reaction (qRT-PCR) at 6 d (hBMSCs only), 11 d, and 20 d (hBMSCs only and hBMSCs+HUVECs coculture) time points as previously described.[32] The relative expression of osteogenic genes *RUNX2a*, *OSTEOCALCIN*, and *DLX5* was analyzed with qRT-PCR at 11 d and 20 d time points (hBMSCs only and hBMSCs+HUVECs coculture). The data was normalized to the expression of a housekeeping gene *RPLP0* (human acidic ribosomal phosphoprotein P0), and the calculations were conducted using a previously described mathematical model.[33] For *vWF* and *PECAM*, the QuantiTect primer assays were used (Qiagen, Hilden, Germany). The primer sequences and accession numbers for *RPLP0* and osteogenic genes *RUNX2a*, *OSTERIX*, and *DLX5* are listed in Table 1. The qRT-PCR mixture contained cDNA, primers, and SYBR Green PCR Master Mix (Applied Biosystems). The reactions were carried out with an ABIPRISM 7300 sequence detection system, and the results were analyzed with AbiPrism 7300 sequence detection system software (Applied Biosystems).

Immunocytochemical Staining. The expression of endothelial marker proteins vWF and CD31 (the product of the *PECAM* gene) was characterized with immunocytochemical staining after 13 d and 20 d of culture (hBMSCs only and hBMSCs+HUVECs coculture). The protocol was conducted as previously described.[32] The following primary antibodies were used: CD31 monoclonal mouse antihuman antibody (dilution 1:20, Dako, Agilent, Santa Clara, CA) and rabbit polyclonal anti-vWF antibody (dilution 1:100, Abcam). The primary antibodies were incubated overnight at +4 °C. The secondary antibodies goat antimouse Alexa Fluor 488 (for CD31 staining; dilution 1:200; Thermo Fisher Scientific) and goat antirabbit Alexa Fluor 568 (for vWF staining; dilution 1:500; Thermo Fisher Scientific) were incubated for 1 h at room temperature. The images were acquired with an Olympus IX51 phase contrast microscope with fluorescence optics and Olympus DP30BW camera.

Statistical Testing. Statistical testing was conducted with SPSS version 23 (IBM, Armonk, NY) using a nonparametric test due to small sample size. The effects of the scaffolds on cell viability, cell amount, ALP activity, and gene expression were compared using the Kruskal–Wallis test with Mann–Whitney U post hoc test and Bonferroni correction. The results were considered significant when $p < 0.05$. The cell culture experiments were repeated with 1 donor line with 3 or 4 parallel samples ($n = 3$ or $n = 4$). However, most likely due to the small sample size, no significant differences between the test groups were detected.

RESULTS

Scaffolds Fabrication via DIW and Morphological Features. In this work, we used a viscous solution of PCL dissolved in acetone as the carrier phase to disperse the BaG microparticles to formulate a homogeneous ink. Up to 50% of BaGs calculated as the dry weight in PCL/BaG could be mixed into the ink with the aid of orbital mixing. In DIW, the printing nozzle was immersed in a cold ethanol bath, and the printed struts solidified as extruded due to the solubility change of PCL in acetone (soluble) and in ethanol (insoluble).

Figure 1 presents the optical and morphological images of the PCL/S53P4–Cu1 scaffolds with various compositional ratios at

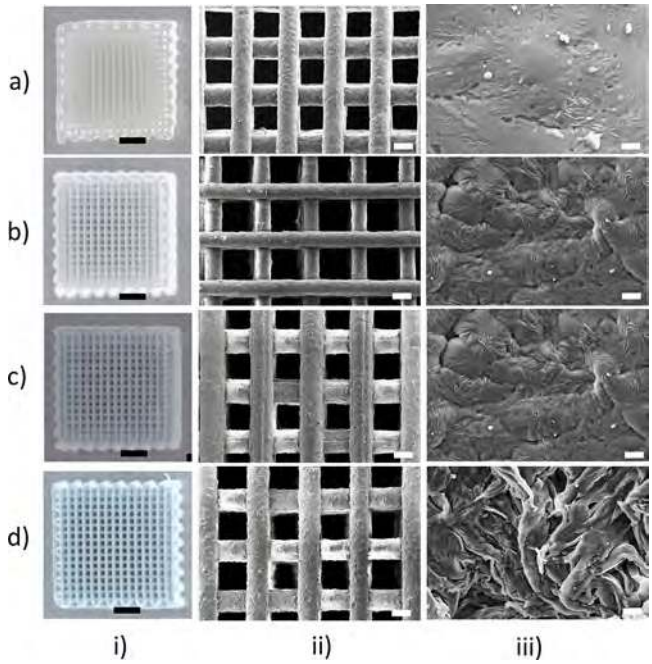

Figure 1. Optical images (column i) and SEM images of the scaffolds (column i and column ii) of PCL ($d = 400\ \mu m$) (row a), PCL:S53P4–Cu1 = 4:1 ($d = 400\ \mu m$) (row b), PCL:S53P4–Cu1 = 2:1 ($d = 400\ \mu m$) (row c), and PCL:S53P4–Cu1 = 1:1 ($d = 400\ \mu m$) (row d). Scale bars: 2 mm (i), 200 μm (ii), 2 μm (iii).

4:1, 2:1, or 1:1 (wt %). Overall, the well-defined layouts of the struts were obtained in all the scaffolds, as seen in the first two columns. After the solvent exchange and drying, the printed scaffolds shrank compared to the designed model, more in the *z*-axis than the *x*- and *y*-axes (Table 2). The gravitational force was

DOI: 10.1021/acsbiomaterials.9b00105
ACS Biomater. Sci. Eng. 2019, 5, 4496–4510

Table 2. Structural Parameters of 3D Printed Scaffolds of PCL/S53P4−Cu1

scaffold	dimension (mm × mm × mm) mean ± SEM	axial shrinkage (%)	strut diameter (μm) mean ± SEM	spacing between struts (μm) mean ± SEM	BaG content in composite as revealed by TG[a]
PCL	8.65 (±0.03) × 8.72 (±0.02) × 3.20 (±0.03)	13−14% on *x*- and *y*-axes; ∼20% on *z*-axis	229 (±16)	297 (±9)	
PCL:S53P4−Cu1 = 4:1	8.86 (±0.07) × 8.88 (±0.05) × 3.28 (±0.06)	∼11% on *x* and *y*-axes; ∼18% on *z*-axis	207 (±8)	339 (±6)	20.2%
PCL:S53P4−Cu1 = 2:1	9.20 (±0.03) × 9.21 (±0.03) × 3.41 (±0.14)	∼8% on *x* and *y*-axes; ∼15% on *z*-axis	232 (±20)	323 (±12)	32.0%
PCL:S53P4−Cu1 = 1:1	9.58 (±0.01) × 9.61 (±0.01) × 3.49 (±0.01)	∼4% on *x* and *y*-axes; ∼12% on *z*-axis	231 (±3)	337 (±4)	57.4%

[a]Determined from the weight loss in the TG analysis curves as shown in Supporting Information S3.

assumed to cause the higher compaction along the *z*-axis during the solidification. Also, the content of S53P4−Cu1 in the composite affected the shrinkage rate. As seen from Table 2, less shrinkage occurred in the composite containing more BaG microparticles since the shrinkage is mainly caused by the condensation of PCL polymer after the removal of organic solvent. The shrinkage decreased from 13% to 14% for the PCL scaffold to 4% for the composite scaffold of PCL/S53P4−Cu1 = 1:1 on *x*- and *y*-axes while for the *z*-axis the difference in the shrinkage was from 20% compared to 12%. The strut diameter and strut spacing were confined within the range 200−230 μm and 300−340 μm, respectively, after the shrinkage upon solidification. As the content of S53P4−Cu1 in the composites increased, the composites showed a coarser surface morphology as revealed by the SEM images (Figure 1). The increased surface roughness in the composites containing more S53P4−Cu1 microparticles was probably due to the presence of more BaG microparticles that protruded the PCL matrix to a larger extent. In the scaffolds of PCL/S53P4−Cu1 = 2:1 and 1:1, small cavities and even microcracks were seen on the surface, indicating a disruption to the continuous phase of PCL in the struts.

TG analysis confirmed the compositional ratio of S53P4−Cu1 in the composite scaffolds, as displayed in Supporting Information S3 as well as listed in Table 2. The residual content was highly consistent with the inorganic content of BaG in the ink dispersion. Also, the cross-section image of the PCL/S53P4−Cu1 = 2:1 scaffold revealed a moderately homogeneous distribution of BaG microparticles through the PCL matrix (as seen in the SEM image in Supporting Information S3). This indicates that the dispersion of BaG microparticles in viscous PCL solution was rather homogeneous, which consequently facilitated the DIW fabrication of the scaffolds with good textural integrity and high resolution.

Compressive Response of the 3D Scaffolds of PCL and PCL/S53P4−Cu1. In a compressive mode, the mechanical responses of the PCL and PCL/S53P4−Cu1 scaffolds were analyzed. The stress−strain response curves for the scaffolds of PCL and PCL/S53P4−Cu1 = 4:1 and 2:1 with the SS = 400 μm are displayed in Figure 2a. The observed stress−strain response of the scaffolds is typical for the highly porous PCL-based scaffolds reported elsewhere.[26,34,35] Their stress−strain curves are characterized by three different regions: a linear region at lower strain values, suggesting an initial rigid mechanical response, associated with elastic behavior of the scaffolds; a region with lower stiffness; and lastly, a region where a rise of stress with increasing strain is recorded, which is related to densification of the porous structure. Compared with the PCL scaffold, all the composite scaffolds exhibited reinforced mechanical properties as the strains were yielded at higher stress values. The compressive Young's moduli *E* of the scaffolds calculated from the slope of the stress−strain curves are displayed in Figure 2b with respect to the compositional ratio between the PCL and S53P4−Cu1. The PCL scaffold showed an *E* value of 5.9 MPa and a yield stress σ_y (at 0.2% strain) of 0.64 MPa. Among the compositional ratios at 4:1, 2:1, and 1:1 for PCL/S53P4−Cu1, the scaffold of PCL/S53P4−Cu1 = 2:1 exhibited the highest *E* value of 12.5 MPa and yield stress σ_y (at

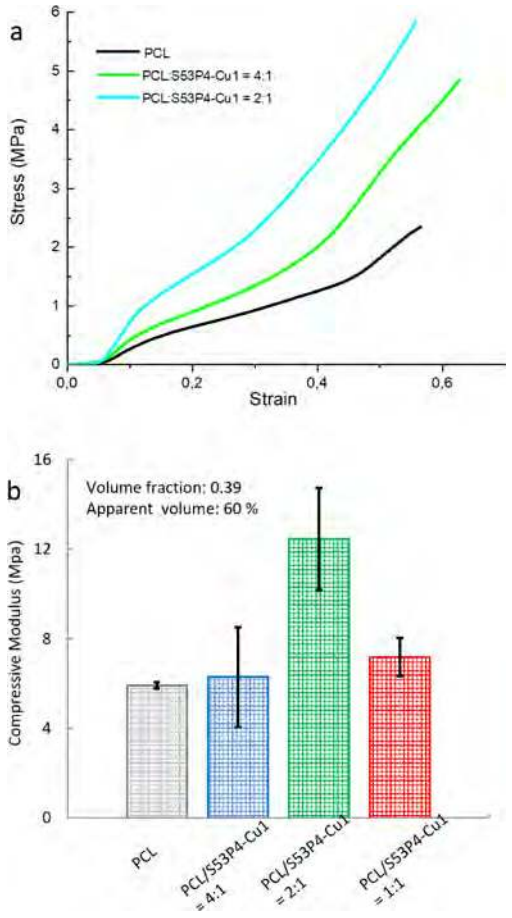

Figure 2. (a) Stress−strain curves for the 3D scaffolds. (b) Compressive Young's modulus vs the compositional ratio of PCL/S53P4−Cu1 in the scaffold. Error bar: SEM.

DOI: 10.1021/acsbiomaterials.9b00105
ACS Biomater. Sci. Eng. 2019, 5, 4496−4510

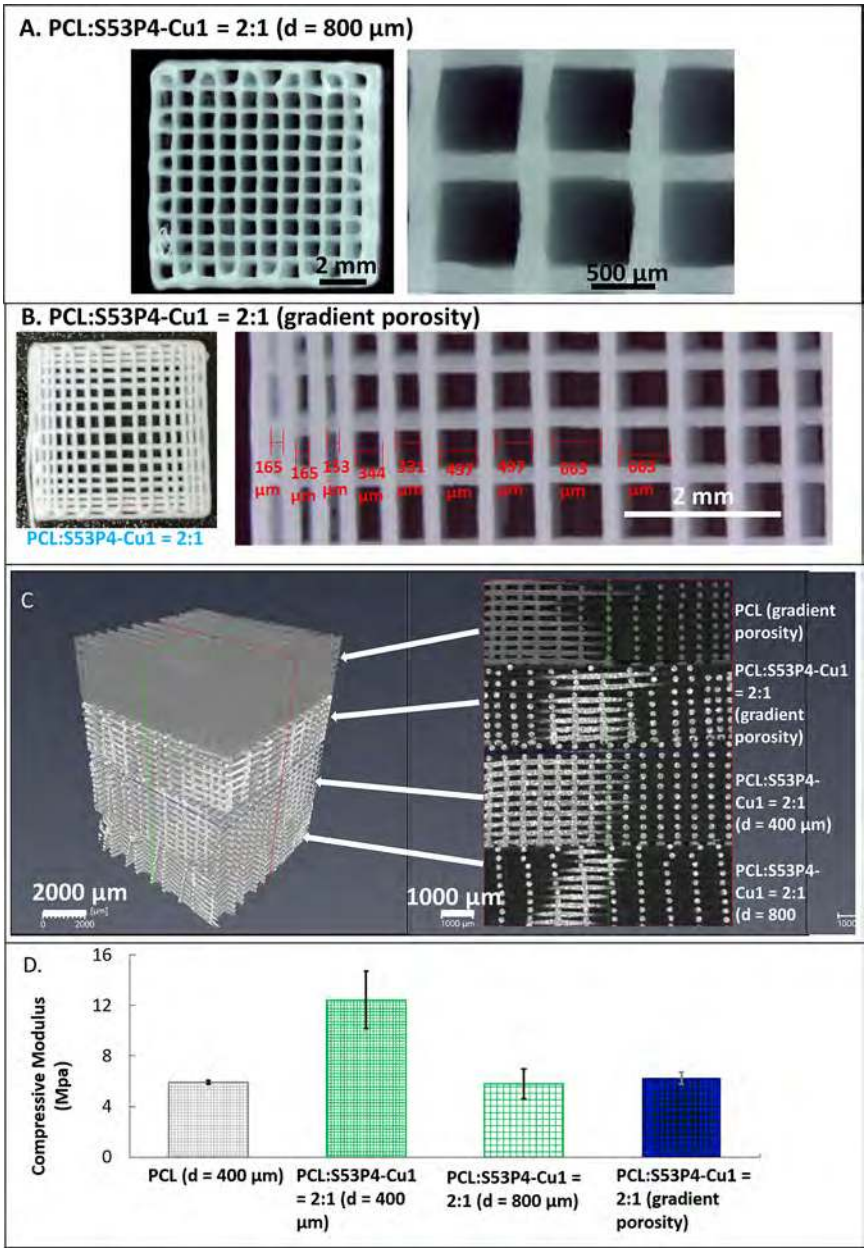

Figure 3. (A) Optical images of the scaffold of PCL/S53P4−Cu1 = 2:1 with strut spacing at d = 800 μm. (B) Optical images of the scaffold of PCL/S53P4−Cu1 = 2:1 with a dense outward gradient porosity. (C) μ-CT images of the scaffolds with different porosity parameter. (D) Young's modulus with respect to various porosity in scaffolds of PCL and PCL/S53P4−Cu1 = 2:1.

0.2% strain) of 1.54 MPa, more than 2 times higher than the PCL scaffold of similar porosity. As revealed by the μ-CT measurements, all the scaffolds printed with SS = 400 μm gave a volume fraction of approximately 0.39 as well as an apparent porosity of 60%. The scaffold of PCL/S53P4−Cu1 = 4:1 demonstrated a similar compressive modulus to the PCL scaffold with an E value of 6.29 MPa, while the scaffold of PCL/S53P4−Cu1 = 1:1 demonstrated an E value of 7.19 MPa, which is lower than that of the scaffold of PCL/S53P4−Cu1 = 2:1. The reduction in mechanical properties of the scaffold of PCL/S53P4−Cu1 = 1:1 can be attributed to the formation of BaG agglomerates, which may result in a heterogeneous dispersion of the inorganic fillers in the PCL matrix, as observed in the SEM images (Figure 1d,iii).

Porosity Control on the Printed Scaffold in DIW. As revealed by the μ-CT measurements, the scaffolds printed with SS = 400 μm gave a volume fraction of about 0.393 as well as an apparent porosity of 60.64%. To demonstrate the precision control of the DIW process over the scaffold porosity with the developed ink system, the scaffolds with the SS = 800 μm (shown in Figure 3A) or with a dense outward gradient porosity (shown in Figure 3B) were, respectively, printed using the ink of the compositional ratio at PCL/S53P4−Cu1 = 2:1. It showed that, after solidification, the scaffolds with SS = 800 μm had the same strut diameters of 232 μm as the scaffolds with SS = 400 μm, but the SS remained around 610 μm. The μ-CT measurements gave a volume fraction of 0.274 with an apparent porosity of 72.53%. In the design of dense outward gradient porosity, the strut spacing was set with a linear change from edge to center on both x- and y-axes. As displayed in Figure 3B, this resulted in an almost linear change of the SS value from 165 to 663 μm in the scaffold after shrinkage.

DOI: 10.1021/acsbiomaterials.9b00105
ACS Biomater. Sci. Eng. 2019, 5, 4496−4510

Table 3. Pore Architecture Parameters in the Printed Scaffold of PCL/S53P4−Cu1 = 2:1

scaffold PCL:S53P4−Cu1 = 2:1	strut diameter (μm) mean ± SEM	spacing between struts (μm) mean ± SEM	volume fraction measured by μ-CT	porosity measured by μ-CT (%)
d = 400 μm	232 (±20)	323 (±12)	0.393	60.64
d = 800 μm	232 (±20)	610	0.274	72.53
gradient porosity	232 (±20)	gradient change	0.261	73.92

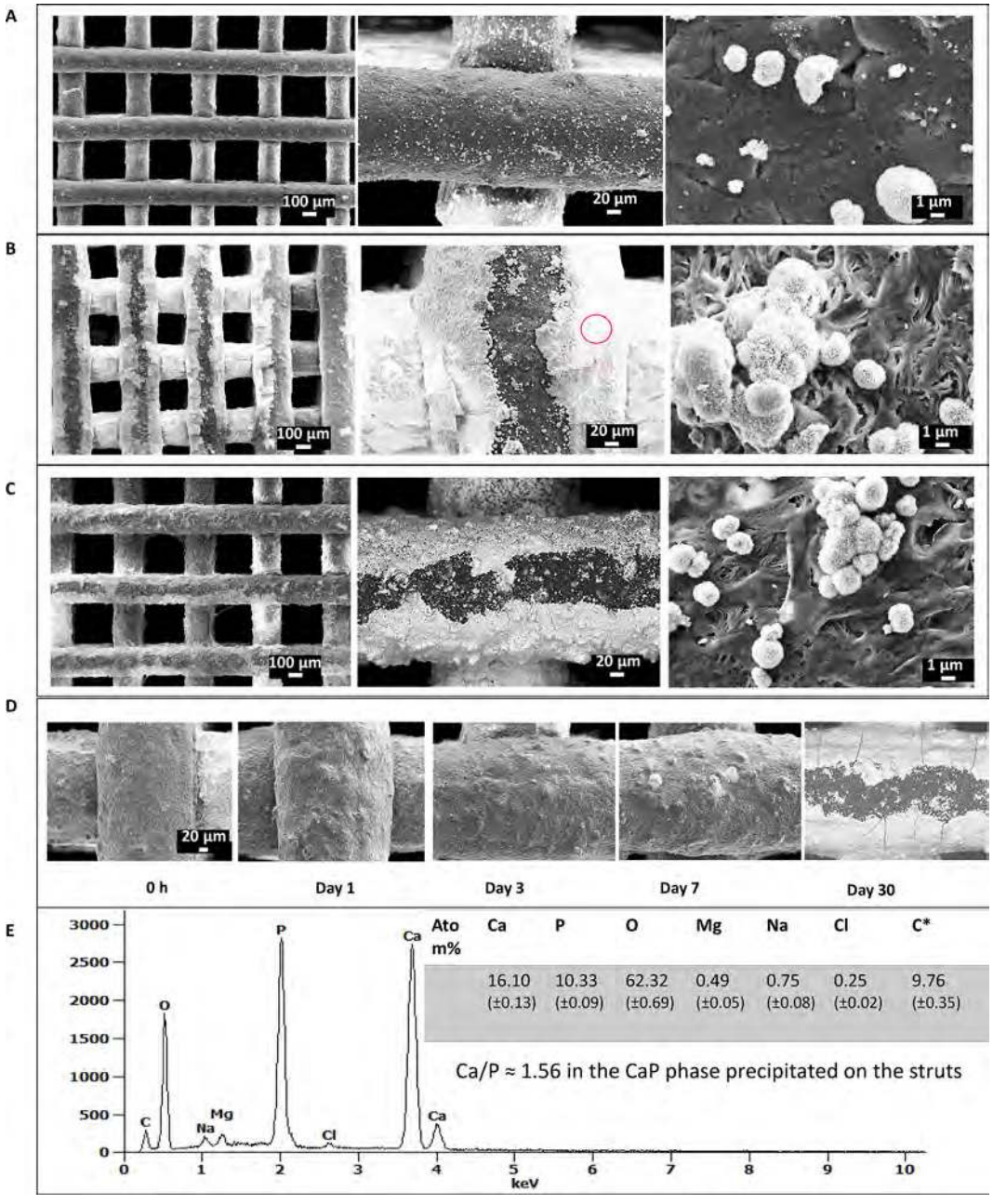

Figure 4. (A) SEM image of the strut surface in the scaffold of PCL/S53P4−Cu1 = 4:1 after 30 days of immersion in SBF in various resolutions. (B) SEM image of the strut surface in scaffold PCL/S53P4−Cu1 = 2:1 after 30 days of immersion in SBF in various resolutions. (C) SEM image of the strut surface in scaffold of PCL/S53P4−Cu1 = 1:1 after 30 days of immersion in SBF in various resolutions. (D) SEM image of the strut surface in scaffold of PCL/S53P4−Cu1 = 2:1 at various immersion time points. (E) EDXA performed on the precipitates on the strut surface in scaffold of PCL/S53P4−Cu1 = 2:1 after 30 days of immersion in SBF.

For the scaffolds with different porosity parameters, the μ-CT image on the left in Figure 3C demonstrates the 3D spatial space inside the printed scaffolds, and the image on the right presents the 2D distribution of struts in the scaffolds. In general, the 3D reconstruction of the scaffolds displayed as the "replicates" in accordance to the CAD designs, indicating good controllability of the developed DIW process. The pore architecture parameters in these scaffolds are summarized with respect to the varied porosity in Table 3. The Young's moduli of these scaffolds were also compared with respect to the porosity in

DOI: 10.1021/acsbiomaterials.9b00105
ACS Biomater. Sci. Eng. 2019, 5, 4496−4510

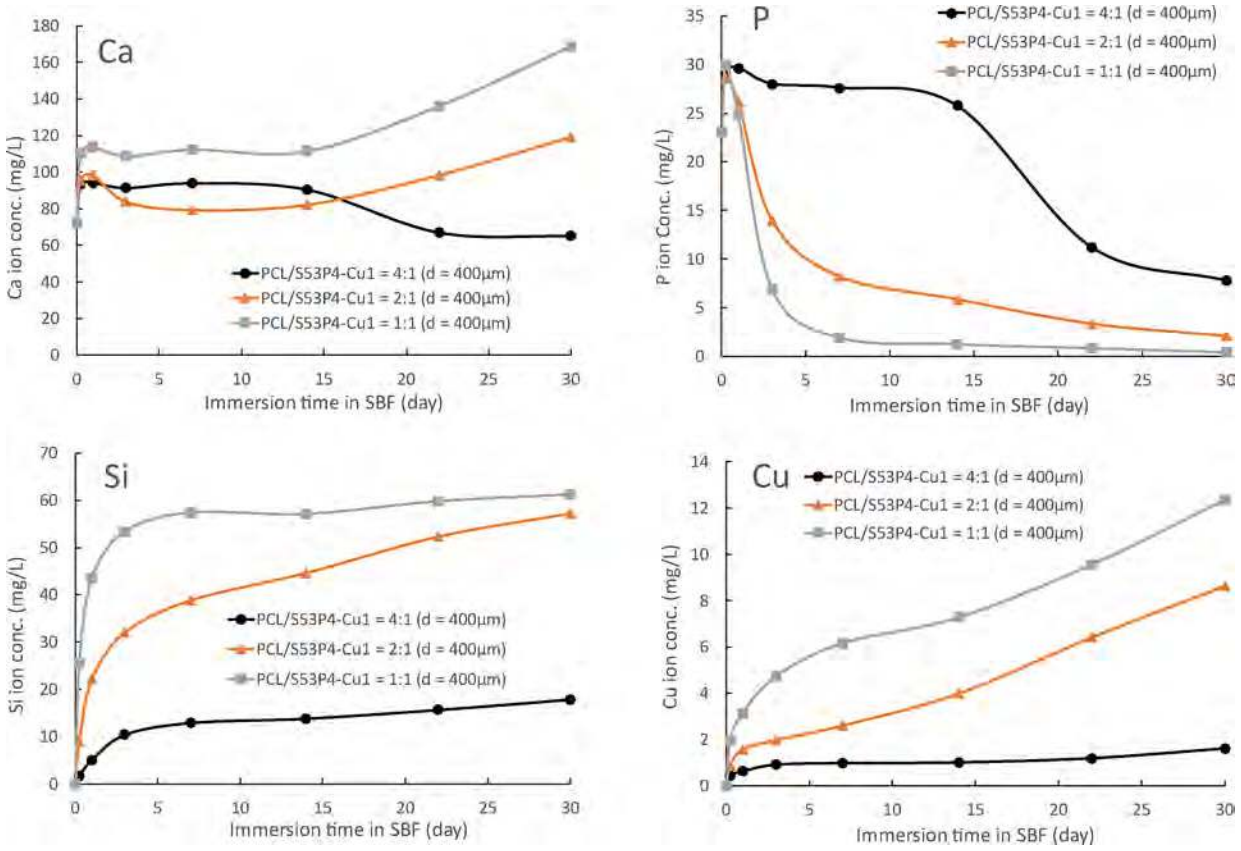

Figure 5. Ion concentration profiles of Ca, P, Si, and Cu ions in SBF with static immersion of PCL/S43P4-Cu1 scaffolds at various compositional ratios.

Figure 3D. Compared with the scaffold with SS = 400 μm, the compressive modulus decreased for both the scaffold with SS = 800 μm and the one with a gradient porosity, as the porosity in both types of scaffolds increased to ~73%. An increase of the total porous volume from 10% to 20% may result in a factor of 4 decrease in the mechanical strength.[36]

Ion Dissolution Profiles and Bioactivity of PCL/Cu-BaG Scaffolds in SBF *in Vitro*. The bioactivity and ion dissolution behaviors of the scaffolds of PCL/S53P4−Cu1 (SS = 400 μm) at various compositional ratios were evaluated in SBF for a total duration of 30 d. Figure 4A−C, respectively, displays the strut surface morphology in the scaffolds of PCL/S53P4−Cu1 = 4:1, 2:1, and 1:1 after static immersion in SBF for 30 d. In the scaffold of PCL/S53P4−Cu1 = 4:1, only small aggregates of calcium phosphate phase (CaP) decorated on the strut surface (Figure 4A), whereas heavy precipitation of CaP formed layers covered the strut surface in the scaffolds of both PCL/S53P4−Cu1 = 2:1 and PCL/S53P4−Cu1 = 1:1 (Figure 4B,C). The CaP precipitate demonstrated a characteristic cauliflower-like morphology consisting of numerous nanoflakes and gave a Ca/P = 1.56 as measured by the EDXA (Figure 4E), which was close to the Ca/P ratio of 1.67 in natural bone minerals, hydroxyapatite. Figure 4D reveals the morphological change of the strut surface in the scaffold of PCL/S53P4−Cu1 = 2:1 at various time points during the SBF immersion. Notable precipitation of the CaP phase on the strut surface was only observed after 7 d of immersion.

By analyzing the ion concentrations in SBF at various time points, the ion dissolution profiles of the scaffolds were acquired. Figure 5 displays the ion dissolution profiles for PCL/S53P4−Cu1 scaffolds with compositional ratios at 4:1, 2:1, and 1:1, all with dimensions of 10 mm (x) × 10 mm (y) × 2 mm (z) and SS = 400 μm defined in DIW. With respect to the dissolution of Si, in all three types of scaffolds a burst release was initially detected within 3 d of immersion, which was most likely associated with the initial dissolution of Cu-BaG particles exposed on the most outer surface. After 3 d, the Cu-BaG dissolution slowed down when the ion diffusion from the inner of the particles might have been hindered by the formed silica-rich layer. Overall, a rather low amount of Si was detected for the scaffold of PCL/S53P4−Cu1 = 4:1 due to the low content of S53P4−Cu1. For the scaffold of PCL/S53P4−Cu1 = 2:1, a continuous release of Si at an almost constant rate was detected for the rest of the immersion period, whereas the Si released from the scaffold of PCL/S53P4−Cu1 = 1:1 reached a saturation level at ~60 mg L^{-1} in SBF after 7 d of immersion. With respect to the dissolution of Cu, in general the release trend was similar to that of Si. A higher concentration of Cu^{2+} was observed in SBF from the scaffold of PCL/S53P4−Cu1 = 1:1 due to the highest burst release in the initial dissolution. The ion concentration profiles of Ca and P in SBF are reflected both by the ion dissolution from the scaffold and by the precipitation of CaP phase on the strut surface. For the scaffold of PCL/S53P4−Cu1 = 4:1, apparent precipitation of CaP was only seen after 14 d of immersion due to the low concentration of Ca^{2+} accumulated in SBF, as indicated by the steep ramp in P concentration. For the scaffolds of PCL/S53P4−Cu1 = 2:1 and PCL/S53P4−Cu1 = 1:1, the CaP precipitation was readily indicated after 1 d of immersion by the steep ramp of P concentration in SBF as shown in Figure 5.

DOI: 10.1021/acsbiomaterials.9b00105
ACS Biomater. Sci. Eng. 2019, 5, 4496−4510

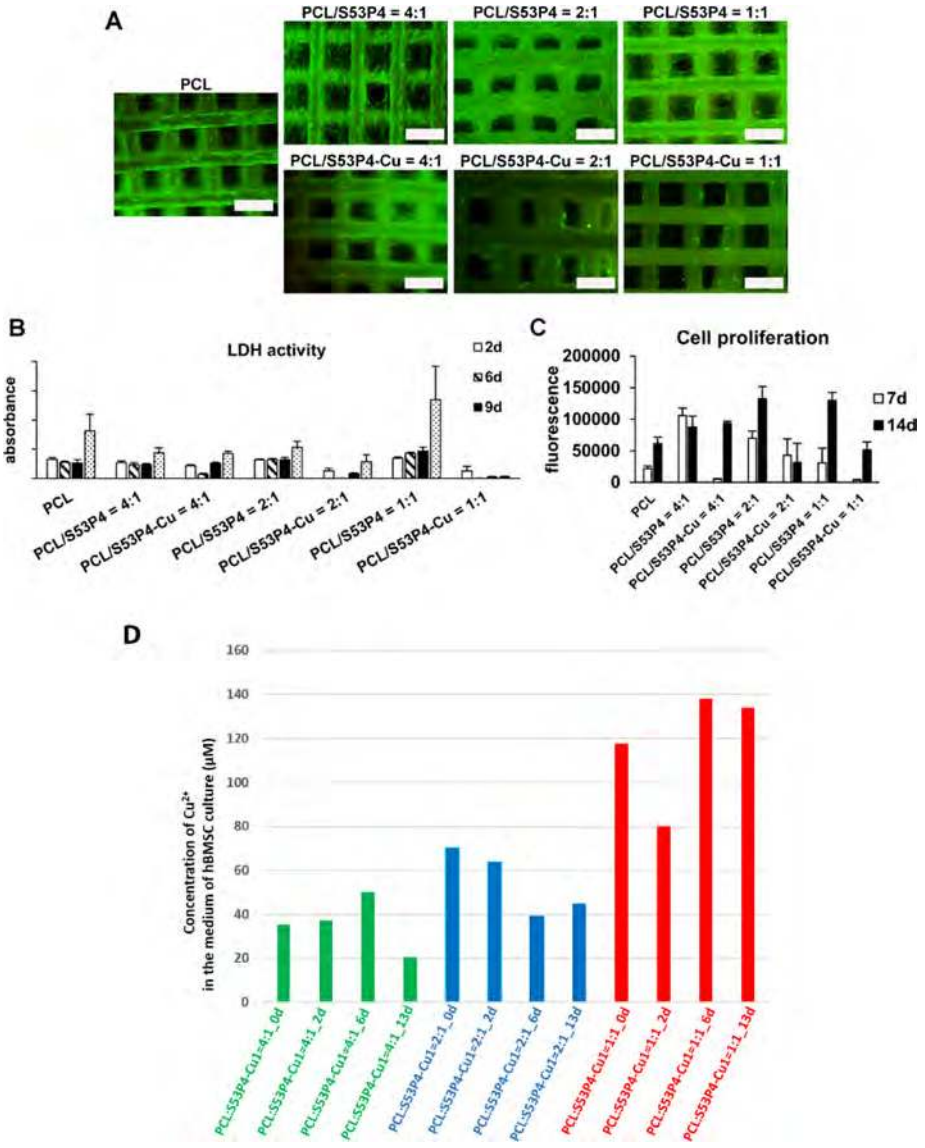

Figure 6. Results concerning viability and proliferation of hBMSCs in scaffolds. (A) Representative images of live/dead staining at the 14 d time point. Live cells are stained green and dead cells red. Scale bars: 500 μm. (B) LDH activity results at 2 d, 6 d, 9 d, and 13 d time points (n = 3, mean + SD). (C) Total DNA amount in samples at 7 d and 14 d time points, indicating hBMSC proliferation (n = 4, mean + SD). (D) ICP-OES analysis results on Cu^{2+} concentration in culture medium at 0 d, 2 d, 6 d, and 13 d time points (n = 1).

hBMSC Culture on the Scaffolds. To determine the viability of hBMSCs on the scaffolds, a qualitative live/dead staining as well as a quantitative LDH activity assay were conducted. As made evident in Figure 6A, the cells were viable on all the materials after 14 d of culture, and the number of dead cells was negligible. Increasing the content of S53P4 in the composite seemed to induce hBMSC proliferation more in comparison to the PCL control. However, apart from the scaffold of PCL/S53P4−Cu1 = 4:1, the high content of S53P4−Cu1 had a clear negative effect on the cell amount.

Cells release LDH enzyme to the culture medium upon cell death associated membrane rupture, making LDH a good quantitative indicator of cell viability. Figure 6B shows the LDH activity levels of the culture medium after 2 d, 6 d, 9 d, and 13 d of culture. Since the medium was changed at each of these time points, the LDH activity values are not cumulative. In general, the LDH activities remained at a relatively low and constant level with all the scaffolds until 9 d, indicating low cytotoxicity of the studied scaffolds. At 13 d the values increased slightly, which is likely due to the high cell density at this point, as observed in the live/dead staining (Figure 6A). Unexpectedly, the amount of Cu^{2+} released from the scaffolds of PCL/S53P4−Cu1 = 2:1 and PCL/S53P4−Cu1 = 1:1 did not induce elevated LDH levels in the culture medium, as expected based on the live/dead staining. Still, cell amount in the S53P4−Cu1-containing scaffolds was clearly less than that in the other samples, thus possibly explaining this observation.

The cell proliferation was quantitatively evaluated at time points of 7 d and 14 d as shown in Figure 6C. The integration of S53P4 in the composite showed an increasing effect on the hBMSC proliferation at both time points and with all the studied BaG contents. Regarding the role of Cu^{2+} released from S53P4−Cu1, the cell proliferation assay was in line with the live/dead staining, indicating the inhibitory effect of the increased concentration of Cu^{2+} on the growth of hBMSCs. Still, despite the very low cell amount on the scaffold of PCL/S53P4−Cu1 =

DOI: 10.1021/acsbiomaterials.9b00105
ACS Biomater. Sci. Eng. 2019, 5, 4496−4510

4:1 at 7 d, the cell amount at 14 d was comparable to that in the scaffold of PCL/S53P4 = 4:1. The Cu^{2+} concentration in the culture medium at time points of 0 d, 2 d, 6 d, and 13 d was further analyzed by ICP-OES, which are presented in Figure 6D with respect to the compositional ratio. During the preincubation in BM for 48 h (0 d at cell seeding), the concentration of Cu^{2+} in the culture medium, respectively, reached 35, 70, and 117 μM released from the scaffolds of PCL/S53P4−Cu1 = 4:1, 2:1, and 1:1. As seen in Figure 6C, the proliferation of hBMSCs on the scaffold of PCL/S53P4−Cu1 = 4:1 was first inhibited at the early time point of 7 d. When the concentration of Cu^{2+} decreased to 20 μM after the culture medium was changed several times, and the dissolution rate of Cu slowed down after the initial burst, the hBMSCs were able to retain their proliferative capacity at the later time point of 14 d, which was comparable to that on the scaffold of PCL/S53P4 = 4:1. However, at both time points of 7 d and 14 d, the proliferation of hBMSCs was restricted on the scaffolds of PCL/S53P4−Cu1 = 2:1 and PCL/S53P4−Cu1 = 1:1 due to the high concentration of Cu^{2+} in the culture media at these time points. Apparently, the concentration of Cu^{2+} is critical for retaining the proliferative capacity of hBMSCs.

To evaluate the early osteogenic commitment of hBMSCs on the scaffolds, ALP activity was quantitatively determined after 7 d and 14 d of culture. As seen in Figure 7, the ALP activity

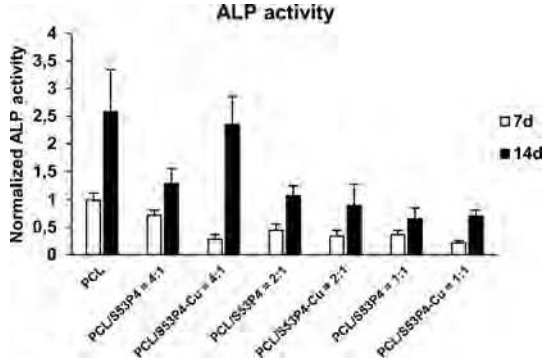

Figure 7. Alkaline phosphatase activity results of hBMSCs in scaffolds at 7 d and 14 d time points. Results are normalized to cell amount (n = 4, mean + SD).

increased on all the materials from 7 d to 14 d, indicating that all the scaffolds supported the early osteogenic differentiation. On one hand, the ALP activity decreased with increasing the BaG content (both for S53P4 and S53P4−Cu1), and the highest values were detected on the PCL control. On the other hand, a higher ALP activity was observed in the scaffold of PCL/S53P4−Cu1 = 4:1 in contrast to the scaffold of PCL/S53P4 = 4:1.

hBMSCs and hBMSCs+HUVECs Coculture on the Scaffolds. The ability of the PCL/BaG and PCL/Cu-BaG scaffolds to support the vascularization in both hBMSC culture and hBMSC+HUVEC coculture was analyzed by immunocytochemical staining of the endothelial proteins CD31 and vWF after 13 d and 20 d of culture. Moreover, the expression of these two markers was also evaluated in gene level with the qRT-PCR after 6 d, 11 d, and 20 d of culture. Due to the observed inhibitory effect of the scaffold of PCL/S53P4−Cu1 = 2:1 and PCL/S53P4−Cu1 = 1:1, only the scaffold of PCL/S53P4−Cu1 = 4:1 was chosen for the coculture experiments, along with the PCL scaffold as a control to the composite scaffold and the PCL/S53P4 = 4:1 scaffold as a Cu-free composite control. As seen in Figure 8A,B, elevated production of CD31 protein was

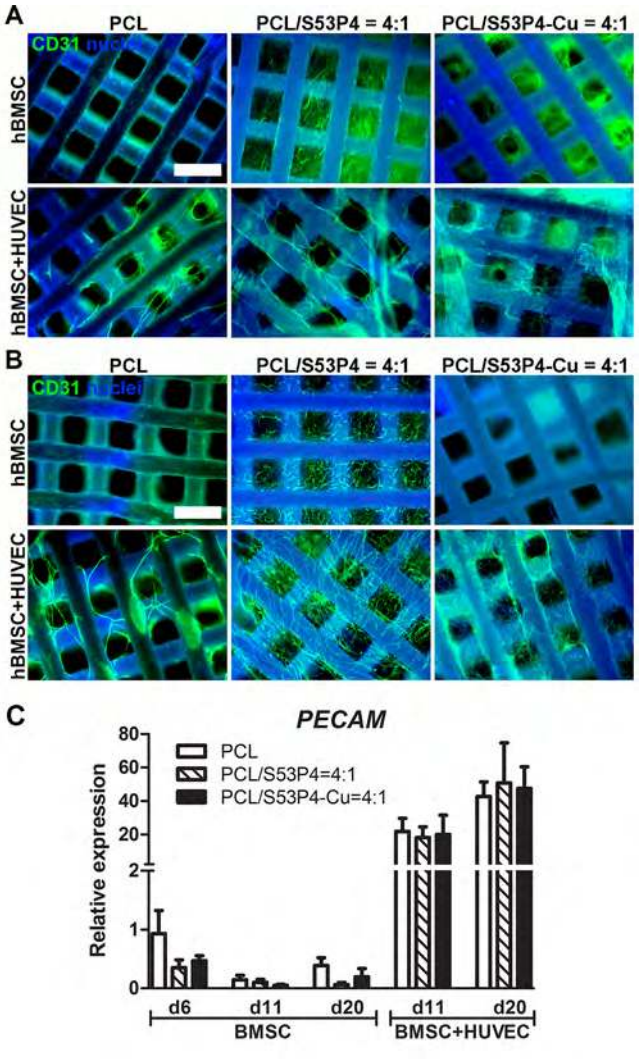

Figure 8. Immunocytochemical staining of endothelial marker protein CD31 (stained green) in hBMSCs and hBMSCs+HUVECs cultured in scaffolds at (A) 13 d and (B) 20 d time points. Nuclei are stained blue; scale bars: 500 μm. (C) Gene expression results of endothelial marker gene *PECAM* in hBMSC and hBMSC+HUVEC cultures at 6 d, 13 d, and 20 d time points. Results are expressed relative to hBMSCs cultured for 6 days on PCL scaffold (n = 3, mean + SD).

observed on all the scaffolds in the coculture. Importantly, extensive tubule formation was clearly visible. On the PCL scaffold, the tubular structures were thick but relatively sparse, whereas a denser network of thinner tubules was formed on the S53P4-containing scaffolds. However, the scaffold of PCL/S53P4−Cu1 = 4:1 did not stimulate tubule formation to a higher extent when compared with the Cu-free scaffold of PCL/S53P4 = 4:1. Notably, S53P4 in the composite scaffolds also stimulated the CD31 production in the hBMSC culture without HUVECs, although no tubular structures were detected. On the gene level, *PECAM* was notably upregulated in the coculture when compared with the hBMSC culture, but no clear differences among the material groups could be detected (Figure 8C). Still, in the coculture model, the expression increased from 11 d to 20 d in all the groups.

DOI: 10.1021/acsbiomaterials.9b00105
ACS Biomater. Sci. Eng. 2019, 5, 4496−4510

The production of vWF was in line with the immunological staining of CD31 as made evident in Figure 9. Tubular structures

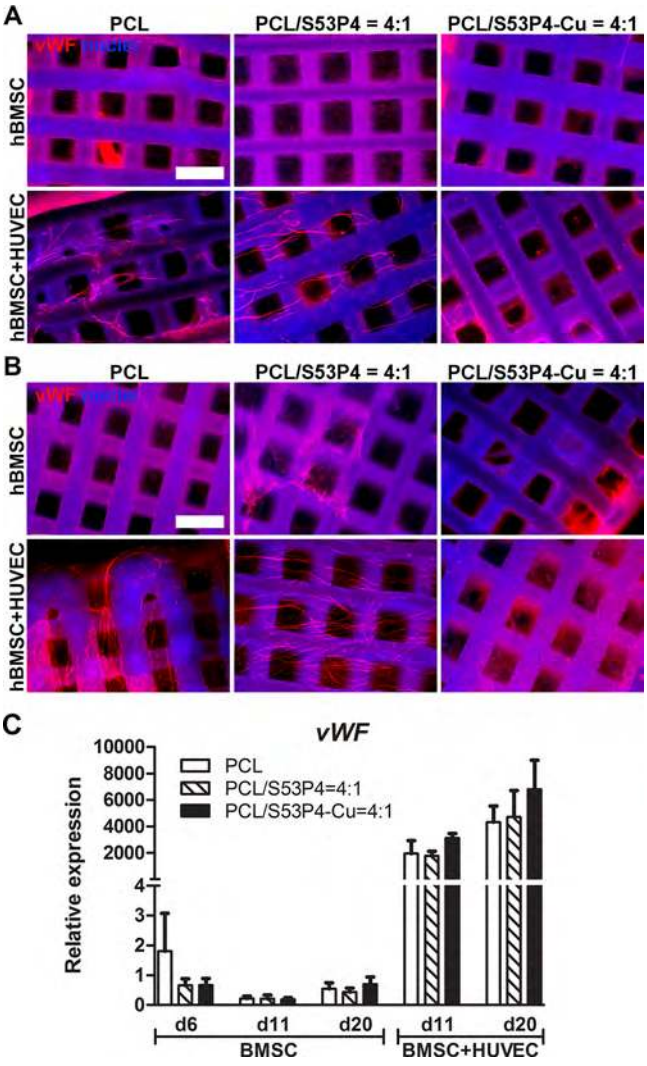

Figure 9. Immunocytochemical staining of endothelial marker protein vWF (stained red) in hBMSCs and hBMSCs+HUVECs cultured in scaffolds at (A) 13 d and (B) 20 d time points. Nuclei are stained blue; scale bars: 500 μm. (C) Gene expression results of endothelial marker gene *vWF* in hBMSC and hBMSC+HUVEC cultures at 6 d, 13 d, and 20 d time points. Results are expressed relative to hBMSCs cultured for 6 days on PCL scaffold (n = 3, mean + SD)

were evident in the coculture on the scaffold of PCL and the scaffold of PCL/S53P4 = 4:1 at 13 d (Figure 9A), and their amount had clearly increased at 20 d especially on the scaffold of PCL/S53P4 = 4:1 (Figure 9B). Still, the Cu^{2+} released from the scaffold of PCL/S53P4−Cu1 = 4:1 did not stimulate the vWF production or the tubular structure formation. There was a low level of vWF production also in the culture of hBMSC alone, but no tubular structures were observed. The relative *vWF* gene expression followed a highly similar pattern as *PECAM*; elevated expression levels were observed in the coculture, but the differences among the material groups were minimal (Figure 9C). In the coculture, the *vWF* gene expression increased from 11 d to 20 d, and at both time points the expression level was slightly higher in the scaffold of PCL:S53P4−Cu1 = 4:1 when compared with the other groups.

The effect of PCL, PCL/S53P4 = 4:1, and PCL/S53P4−Cu1 = 4:1 scaffolds on osteogenic differentiation in both hBMSC culture and hBMSC+HUVEC coculture was analyzed by qRT-PCR of osteogenic marker genes *RUNX2a*, *OSTEOCALCIN*, and *DLX5* after 11 d and 20 d of culture. The early osteogenic marker gene *RUNX2a* expression was elevated in hBMSCs when cultured in the scaffolds of PCL and PCL/S53P4−Cu1 = 4:1 in comparison to the scaffold of PCL/S53P4 = 4:1 at both time points (Figure 10A). In contrast, in hBMSC+HUVEC culture the scaffold of PCL/S53P4 = 4:1 promoted *RUNX2a* expression more at both time points in comparison to the other two scaffolds. The scaffold of PCL/S53P4−Cu1 = 4:1 seemed to have a decreasing effect on both *OSTEOCALCIN* and *DLX5* expression, whereas the scaffold of PCL/S53P4 = 4:1 elevated their expression at both time points and both culture setups (Figure 10B,C). Altogether, the expression of the osteogenic genes was more pronounced in hBMSC culture in contrast to the coculture setup.

DISCUSSION

Tuning the Architecture Parameters and Balancing the Mechanical Strength of PCL/BaG Scaffolds. The architecture parameters in scaffolds, including pore size and distribution, pore interconnectivity, and void volume, are important aspects to consider in designing TE scaffolds.[36] Optimal porosity in a scaffold allows the migration and proliferation of seeded cells, as well as the formation of a vascular network. A high porosity, greater than 80%, is desirable to enhance the osteogenesis.[36] An interconnected architecture of macropores has a decisive effect for the ingrowth of new bone, especially in long-term tissue interface maintenance. A pore size greater than 300 μm is of importance for the osteogenesis to occur as well as for the development of the vascularization network through the TE construct.[37,38] Furthermore, the TE scaffolds shall incorporate a similar structural complexity as the native tissues, which typically have a gradient porous structure.[39] The gradient porosity enables specific cell migration during tissue regeneration. The gradient porosity is also required for the treatment of articular cartilage defects in osteochondral TE.[37,40]

In this work, we have successfully fabricated 3D printed scaffolds with different pore sizes and porosities, as well as a gradient porous structure (Figure 3). In the early osteogenic differentiation culture of hBMSCs, the scaffolds of PCL/S53P4 = 2:1 and PCL/S53P4−Cu1 = 2:1 with different porosity parameters (SS = 400 μm, SS = 800 μm, and gradient porosity as in Figure 3B) were evaluated in terms of cell viability and proliferative capability. However, no significant differences were observed among the tested groups as shown in Supporting Information S4. As indicated by this set of data, the pore size ranging from 167 to 667 μm supports the proliferation of hBMSCs well.

TE scaffolds should have matching mechanical performance to ensure their mechanical integrity during the surgical implantations and to replenish the bone functions during the healing process. The modulus of the human cancellous bones varies in the range 10−1000 MPa with respect to the apparent density of the bone.[41] In this work, we have fabricated scaffolds with 60% apparent porosity, and the highest compressive modulus of 12.5 MPa was measured for the scaffolds of PCL/S53P4−Cu1 = 2:1 with SS = 400 μm. This has determined that the composite scaffolds fabricated by this method are appropriate for the non-load-bearing sites in bone TE. Nevertheless, changing porosity and pore size also resulted in

DOI: 10.1021/acsbiomaterials.9b00105
ACS Biomater. Sci. Eng. 2019, 5, 4496−4510

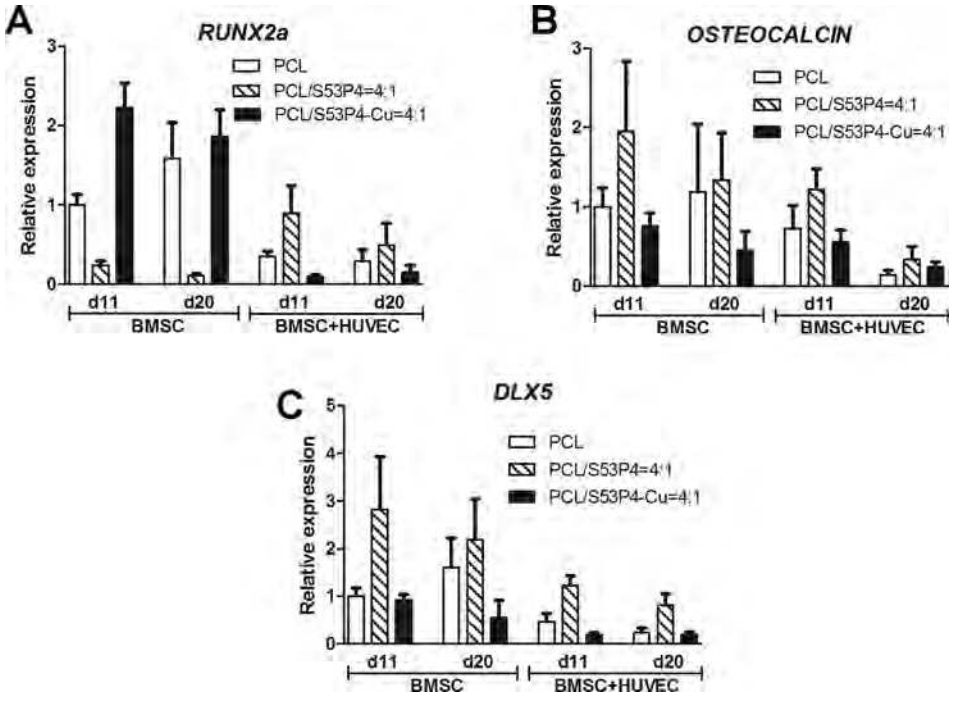

Figure 10. Gene expression results of osteogenic marker genes (A) *RUNX2a*, (B) *OSTEOCALCIN*, and (C) *DLX5* in hBMSC and hBMSC+HUVEC cultures at 13 d and 20 d time points. Results are expressed relative to hBMSCs cultured for 11 days on the PCL scaffold (n = 3, mean + SD).

changes in the mechanical properties, as it changes the density and the structural integrity of the scaffolds (as seen in Figure 3C). However, to achieve modulus in a much higher range, an alternative fabrication strategy and/or reinforcing component need to be considered to enhance the mechanical properties in future studies.

Effect of Cu^{2+} Released from BaG on hBMSCs and HUVECs. The surface reactions occurring on BaG involve ionic dissolution of critical concentrations of soluble Si, Ca, P, and Na ions. These ions give rise to both intracellular and extracellular responses in cells at the interface of the glass. The key phenomenon is the controlled release rates of ionic dissolution products, especially the critical concentrations of soluble Si and Ca ions. For example, 15−30 ppm of soluble Si and 60−90 ppm of soluble Ca ions are needed for osteoconduction or osteostimulation.[42] In the PCL/BaG composite, the primary role of BaG is to release the biologically active ions at the concentrations and rates needed for supporting cell proliferation and differentiation. As discussed in the Results section, the ion concentrations measured in SBF within 30 days were mainly from the dissolution of Cu-BaG microparticles exposed on the most outer strut surface since the degradation of PCL under physiological conditions is rather slow due to the low hydrolytic reactivity of PCL itself (expected to last for years).[43] Above all, the release of inorganic ions from these PCL/S53P4−Cu1 scaffolds can sustain over an extended period.

The physiologically relevant effects of Cu^{2+} as therapeutic ions, such as the antimicrobial properties, have been previously examined by applying the composite of PCL/Cu-BaG nanoparticles as an anticorrosive surface coating onto magnesium implants, as reported by Yang et al.[20] Comparatively, doping of Cu into S53P4 was strategically set to release the Cu^{2+} locally for its therapeutic effect on promoting the angiogenesis in the present study. However, the specific mechanisms of Cu^{2+} affecting the cellular interactions in hBMSCs and HUVECs are complex as indicated by our results. The ion dissolution products of S53P4 are not expected to greatly impact the proliferation of hBMSCs, as suggested in previous studies.[22,44] Regarding the proliferation and differentiation of hBMSCs, the surface wettability is also a key parameter for consideration. Feasibly, the hydrophilic BaG particulates alter the surface hydrophilicity in the composite struts in contrast to the hydrophobic PCL struts. The hydrophilic properties of biomaterials as bone substitutes are important for the induction of early cell attachment and growth.[45] Regarding the role of Cu^{2+} released from the S53P4−Cu1, the cell proliferation results were in line with the live/dead staining results, indicating that a high concentration of Cu^{2+} has an inhibitory effect on the hBMSC proliferation. The generation of reactive oxygen species is one of the main mechanisms by which the Cu^{2+} elicits cytotoxicity in cell monolayers *in vitro*. As recently investigated by Weng et al.,[22] a dose- and exposure-duration-dependent cytotoxicity of Cu^{2+} released from the nanofibers of Cu-BaG was also confirmed for the proliferation of multiple TE-related cell lines, including HUVECs, adipose-tissue-derived stem cells (ADSCs), as well as hBMSCs. In line with our previous results, a high concentration of Cu^{2+} released from the mesoporous Cu-doped BaG microparticles embedded in a nanocellulose hydrogel was cytotoxic for 3T3 fibroblasts.[19] Furthermore, Wu et al. compared mesoporous Cu-BaG scaffolds and their extracts containing varying amount of Cu^{2+} and concluded that a high concentration of Cu^{2+} significantly reduced the hBMSC proliferation.[18] In our study, the highest Cu^{2+} concentration in the culture medium varied from 50 μM (the scaffold of PCL:S53P4−Cu1 = 4:1) to 140 μM (the scaffold of PCL:S53P4−Cu1 = 1:1), and these levels are still less than the 100 mg mL^{-1} being equivalent to the 157 μM level, at which Wu et al. concluded that the Cu^{2+} inhibited the hBMSC growth.[18] According to the proliferation analysis, the hBMSCs retained their proliferative capacity when the concentration of Cu^{2+} was maintained under 20 μM. In a previous study, the Cu^{2+} concentration at 50 μM diminished the proliferate rate of

DOI: 10.1021/acsbiomaterials.9b00105
ACS Biomater. Sci. Eng. 2019, 5, 4496−4510

hBMSCs.[46] In the present study, the cell culture was carried out in a static model while the culture medium was only changed on fixed intervals. Under such conditions, the Cu^{2+} released from the scaffold has accumulated between medium changes. Depending on the content of S53P4−Cu1 in the composite, the accumulated Cu^{2+} showed a dose-dependent cytotoxicity on the proliferation of hBMSCs. Obviously, the concentration of Cu^{2+} is critical for retaining the proliferative capacity of hBMSCs.

All the scaffolds supported the ALP activity of hBMSCs, although the increase in the BaG or Cu-BaG content had a decreasing effect on the ALP activity. Previously, it was shown that the ALP activity of hBMSCs slightly increased as the Cu^{2+} concentration rose, however, the difference was not significant.[18] Also, the addition of Cu in BaG did not have a significant effect on the ALP activity of hBMSCs cultured in the Cu-doped 45S5 BaG scaffolds.[47] The high level of ALP activity may not be as important in the osteogenic differentiation as the fact that there is a clear level of ALP activity in samples, ensuring the presence of Pi and decreasing the concentration of pyrophosphate, to allow mineralization.[32] The osteogenic differentiation of hBMSCs was also analyzed by qRT-PCR in hBMSC culture and hBMSC+HUVEC coculture setups with the scaffolds of PCL, PCL:S53P4 = 4:1, and PCL:S53P4−Cu1 = 4:1. Interestingly, in the hBMSC culture setup the Cu-containing scaffold induced the expression of early osteogenic marker gene *RUNX2a* notably in contrast to the scaffold of PCL:S53P4 = 4:1. *RUNX2* expression is essential in the early differentiation of MSCs into osteoblastic lineage.[48] However, in order for the differentiation to proceed, the expression of *RUNX2* needs to decline, as high expression of *RUNX2* has been shown to inhibit osteoblast maturation keeping the cells in a premature stage.[48] Therefore, the high expression of *RUNX2a* as late as at 20 d combined with the low expression of late osteogenic marker genes *OSTEOCALCIN* and *DLX5* in the scaffold of PCL:S53P4−Cu1 = 4:1 is not optimal for osteogenic differentiation. Osteocalcin is only expressed in the late phase of osteogenic differentiation, and *DLX5* is an important activator of several osteogenic genes during maturation and mineralization phases.[49,50] The gene expression of *OSTEOCALCIN* and *DLX5* was higher in the scaffold of PCL:S53P4 = 4:1 in comparison to the scaffold of PCL:S53P4−Cu1 = 4:1 at both time points indicating the negative effect of Cu^{2+} on osteogenic differentiation of hBMSCs. In line with this, Li et al. demonstrated that Cu^{2+} ions inhibited the osteogenesis of rat BMSCs *in vitro*.[51] Furthermore, they showed that Cu^{2+} ions inhibited collagen formation and accumulation of collagen type I while inducing vascular formation *in vivo*. In contrast to OM supplemented hBMSC cultures, the cocultures were supplemented with EGM-2, which explains the lower expression of osteogenic genes in the coculture. Also, the expression of the osteogenic genes seemed to go down from 11 d to 20 d in the coculture setup.

According to the immunocytochemical staining of CD31 and vWF, both scaffolds of PCL:S53P4 = 4:1 and PCL:S53P4−Cu1 = 4:1 induced the secretion of these endothelial proteins and supported the formation of a denser tubular network in both hBMSC and hBMSC+HUVEC cultures in contrast to the PCL scaffold. Similarly, 45S5 BaG has been shown to support the formation of a tubular network in fibroblast and endothelial cell cultures.[14] Also, the S53P4 dissolution products have previously been reported to increase the VEGF secretion of human fibroblasts.[47] The secretion of both CD31 and vWF was stronger in the coculture setup in comparison to the hBMSC culture. In line with this, the Cu-doped 45S5 BaG scaffolds have been demonstrated to stimulate the secretion of VEGF and the formation of tubular networks in a coculture of hBMSCs with human dermal microvascular endothelial cells.[47] Interestingly, they also noticed that the Cu^{2+} alone did not increase the secretion of VEGF in these endothelial cells, but the presence of hBMSCs was also needed.[47] As expected, the gene expression of endothelial genes *PECAM* and *vWF* was notably higher in the coculture setup in comparison to the hBMSC culture with all the scaffolds (PCL, PCL:S53P4 = 4:1, and PCL:S53P4−Cu = 4:1). As several previous studies have suggested that the Cu^{2+} ions have an inductive effect on vascularization, we would have expected to see a more pronounced difference between the scaffolds of PCL:S53P4 = 4:1 and PCL:S53P4−Cu1 = 4:1.[18,19,47] However, only the gene expression of *vWF* in the coculture setup was slightly higher in the Cu-containing scaffold of PCL:S53P4−Cu1 = 4:1 in contrast to the scaffold of PCL:S53P4 = 4:1. These conflicting results may be related to the different experimental design on the Cu-mediated angiogenic or cytotoxic effect, such as the BaG composition, used cell type, or medium supplements. However, we may speculate whether the S53P4 BaG itself promotes angiogenesis, and the addition of Cu^{2+} that was released from the scaffold of PCL:S53P4−Cu1 = 4:1 does not suffice to produce observable differences in tubular network formation. A similar finding was also reported in an *in vivo* evaluation of the angiogenetic effect of the Cu-doped 45S5 scaffolds in the AV loop model: a tendency toward an increased vascularization in the Cu-doped BaG group compared to the plain BaG group was observed in μ-CT and histological evaluations, but no statistical difference in vascularization could be measured between both groups.[52] Altogether, the PCL:S53P4 = 4:1 and PCL:S53P4−Cu1 = 4:1 scaffolds supported the vascularization and tubular formation in the coculture setup; however, the angiogenic effect of Cu^{2+} was not notable in contrast to the PCL/BaG composite. The key point to consider for future experimental design is to optimize the Cu^{2+} release and prevent the accumulation of Cu^{2+} in the culture medium, for instance, by using a dynamic culture system that would also simulate the *in vivo* environments better.

CONCLUSIONS

Using a viscous solution of PCL in acetone as the carrier phase for BaG microparticles to achieve a homogeneous ink in combination with the solidification of PCL in ethanol has enabled the DIW fabrication of the PCL/BaG composite scaffolds. Because of the excellent homogeneity of the DIW ink as prepared, the mechanical properties of the composite scaffolds were enhanced, compared to the PCL scaffold. The DIW technique allows a precise control of the scaffold architecture with high resolutions. The reinforced scaffolds of PCL/S53P4−Cu1 at various compositional ratios and with a strut diameter around 230 μm as well as an apparent porosity of 60% showed a compressive Young's modulus in the range 7−13 MPa. This indicates that the scaffolds would be appropriate to be used for non-load-bearing sites in bone TE. The bioactivity of S53P4−Cu1 in the composite scaffolds was confirmed by the CaP precipitation in SBF *in vitro*. The PCL/S53P4−Cu1 scaffolds as fabricated were able to provide a sustained release of biologically relevant inorganic ions over an extended period. The high content of S53P4−Cu1 in the scaffolds of PCL/S53P4−Cu1 = 2:1 and PCL/S53P4−Cu1 = 1:1 inhibited the proliferation of hBMSCs. However, in the scaffold of PCL/S53P4−Cu1 = 4:1, the hBMSCs retained their proliferative

DOI: 10.1021/acsbiomaterials.9b00105
ACS Biomater. Sci. Eng. 2019, 5, 4496−4510

capacity at a delayed culture time. Furthermore, the rising BaG and Cu content in the composite had a decreasing effect on ALP activity in hBMSCs. The PCL:S53P4 = 4:1 scaffold supported the osteogenic differentiation of hBMSCs whereas the addition of Cu suppressed the osteogenic effect of the composite. The scaffolds of PCL:S53P4 = 4:1 and PCL:S53P4−Cu1 = 4:1 supported the vascularization and tubule formation in the hBMSC+HUVEC coculture setup. Unexpectedly, the Cu^{2+} released from the scaffold of PCL:S53P4−Cu1 = 4:1 did not have an apparent effect on the tubule formation in comparison to the scaffold of PCL:S53P4 = 4:1.

■ ASSOCIATED CONTENT

Supporting Information

The Supporting Information is available free of charge on the ACS Publications website at DOI: 10.1021/acsbiomaterials.9b00105.

Concentrations of inorganic ions in the SBF; surface marker expression of hBMSCs and HUVECs; homogeneity investigation of the 3D scaffolds of PCL/Cu-BaG; and cell viability and proliferation on scaffolds with different porosity control parameters (PDF)

■ AUTHOR INFORMATION

Corresponding Author

*E-mail: xwang@abo.fi.

ORCID

Xiaoju Wang: 0000-0002-1728-4164
Miina Ojansivu: 0000-0002-5493-3530
Chunlin Xu: 0000-0003-1860-9669
Jari Hyttinen: 0000-0003-1850-3055
Gordon Wallace: 0000-0002-0381-7273

Author Contributions

#X.W., B.Z.M., and S.P. contributed equally to this study as the cofirst authors. The manuscript was written through contributions of all the coauthors. All the coauthors have given approval to the final version of the manuscript.

Funding

This work is funded by Academy of Finland with the Academy Project Number of 268455.

Notes

The authors declare no competing financial interest.

■ ACKNOWLEDGMENTS

X.W. would like to thank the Academy of Finland for their financial support on her research work. Linus Silvander, Peter Backman, and Luis Bezerra are, respectively, acknowledged for their technical assistance on SEM, TG, and ICP-OES analysis. S.M. would like to thank the Business Finland, the Human Spare Parts Project, the Academy of Finland, and the Competitive State Research Financing of the Expert Responsibility area of Tampere University Hospital for their financial support on the research. The authors thank Ms. Anna-Maija Honkala, Ms. Sari Kalliokoski, and Tampere Imaging Facility, BioMediTech, Faculty of Medicine and Health Technology, Tampere University for technical assistance.

■ REFERENCES

(1) Wang, W.; Yeung, K. W. K. Bone Grafts and Biomaterials Substitutes for Bone Defect Repair: A Review. *Bioactive Mater.* **2017**, *2*, 224−247.

(2) Yu, X.; Tang, X.; Gohil, S. V.; Laurencin, C. T. Biomaterials for Bone Regenerative Engineering. *Adv. Healthcare Mater.* **2015**, *4*, 1268−1285.

(3) Kolk, A.; Handschel, J.; Drescher, W.; Rothamel, D.; Kloss, F.; Blessmann, M.; Heiland, M.; Wolff, K.-D.; Smeets, R. Current Trends and Future Perspectives of Bone Substitute Materials − From Space Holders to Innovative Biomaterials. *J. Craniomaxillofac. Surg.* **2012**, *40*, 706−718.

(4) Oryan, A.; Alidadi, S.; Moshiri, A.; Maffulli, N. Bone Regenerative Medicine: Classic Options; Novel Strategies and Future Directions. *J. Orthop. Surg. Res.* **2014**, *9*, 18.

(5) Tang, D.; Tare, R. S.; Yang, L.-Y.; Williams, D. F.; Ou, K.-L.; Oreffo, R. O. C. Biofabrication of Bone Tissue: Approaches; Challenges and Translation. *Biomaterials* **2016**, *83*, 363−382.

(6) Hench, L. L. The Story of Bioglass. *J. Mater. Sci.: Mater. Med.* **2006**, *17*, 967−978.

(7) Rahaman, M. N.; Day, D. E.; Bal, B. S.; Fu, Q.; Jung, S. B.; Bonewald, L. F.; Tomsia, A. F. Bioactive Glass in Tissue Engineering. *Acta Biomater.* **2011**, *7*, 2355−2373.

(8) Jones, J. R. Review of Bioactive Glass: from Hench to Hybrids. *Acta Biomater.* **2013**, *9*, 4457−4486.

(9) El-Rashidy, A. A.; Roether, J. A.; Harhaus, L.; Kneser, U.; Boccaccini, A. R. Regenerating Bone with Bioactive Glass Scaffolds: A Review of in vivo Studies in Bone Defect Models. *Acta Biomater.* **2017**, *62*, 1−28.

(10) Almubarak, S.; Nethercott, H.; Freeberg, M.; Beaudon, C.; Jha, A.; Jackson, W.; Marcucio, R.; Miclau, T.; Healy, K.; Bahney, C. Tissue Engineering Strategies for Promoting Vascularized Bone Regeneration. *Bone* **2016**, *83*, 197−209.

(11) Mercado-Pagán, Á. E.; Stahl, A. M.; Shanjani, Y.; Yang, Y. Vascularization in Bone Tissue Engineering Constructs. *Ann. Biomed. Eng.* **2015**, *43*, 718−729.

(12) Day, R. M. Bioactive Glass Stimulates the Secretion of Angiogenic Growth Factors and Angiogenesis In Vitro. *Tissue Eng.* **2005**, *11*, 768−777.

(13) Detsch, R.; Stoor, P.; Grunewald, A.; Roether, J. A.; Lindfors, N. C.; Boccaccini, A. R. Increase in VEGF Secretion from Human Fibroblast Cells by Bioactive Glass S53P4 to Stimulate Angiogenesis in Bone. *J. Biomed. Mater. Res., Part A* **2014**, *102A*, 4055−4061.

(14) Gorustovich, A.; Roether, J. A.; Boccaccini, A. R. Effect of Bioactive Glasses on Angiogenesis: A review of In Vitro and In Vivo Evidences. *Tissue Eng., Part B* **2010**, *16*, 199−207.

(15) Sen, C. K.; Khanna, S.; Venojarvi, M.; Trikha, P.; Ellison, E. C.; Hunt, T. K.; Roy, S. Copper-Induced Vascular Endothelial Growth Factor Expression and Wound Healing. *Am. J. Physiol. Heart Circ. Physiol.* **2002**, *282*, 1821−1827.

(16) Gerard, C.; Bordeleau, L.-J.; Barralet, J.; Doillon, C. J. The Stimulation of Angiogenesis and Collagen Deposition by Copper. *Biomaterials* **2010**, *31*, 824−831.

(17) Kornblatt, A. P.; Nicoletti, V. G.; Travaglia, A. The Neglected Role of Copper Ions in Wound Healing. *J. Inorg. Biochem.* **2016**, *161*, 1−8.

(18) Wu, C.; Zhou, Y.; Xu, M.; Han, P.; Chen, L.; Chang, J.; Xiao, Y. Copper-Containing Mesoporous Bioactive Glass Scaffolds with Multifunctional Properties of Angiogenesis Capacity; Osteostimulation and Antibacterial Activity. *Biomaterials* **2013**, *34*, 422−433.

(19) Wang, X.; Cheng, F.; Liu, J.; Smått, J.-H.; Gepperth, D.; Lastusaari, M.; Xu, C.; Hupa, L. Biocomposites of Copper-containing Mesoporous Bioactive Glass and Nanofibrillated Cellulose: Biocompatibility and Angiogenic Promotion in Chronic Wound. *Acta Biomater.* **2016**, *46*, 286−298.

(20) Yang, Y.; Zheng, K.; Liang, R.; Mainka, A.; Taccardi, N.; Judith, A.; Roether, J. A.; Detscha, R.; Goldmann, W. H.; Virtanen, S.; Boccaccini, A. R. Cu-releasing BG/PCL Coating on Mg with Antibacterial and Anticorrosive Properties for Bone Tissue Engineering. *Biomed. Mater.* **2018**, *13*, 015001.

(21) Bari, A.; Bloise, N.; Fiorilli, S.; Novajra, G.; Vallet-Regí, M.; Bruni, G.; Torres-Pardo, A.; González-Calbet, J. M.; Visai, L.; Vitale-Brovarone, C. Copper-Containing Mesoporous Bioactive Glass

DOI: 10.1021/acsbiomaterials.9b00105
ACS Biomater. Sci. Eng. 2019, 5, 4496−4510

Nanoparticles as Multifunctional Agent for Bone Regeneration. *Acta Biomater.* **2017**, *55*, 493−504.
(22) Weng, L.; Boda, S. K.; Teusink, M. J.; Shuler, F. D.; Li, X.; Xie, J. Binary Doping of Strontium and Copper Enhancing Osteogenesis and Agiogenesis of Bioactive Glass Nanofibers while Suppressing Osteoclast Activity. *ACS Appl. Mater. Interfaces* **2017**, *9*, 24484−24496.
(23) Malikmammadov, E.; Tanir, T. E.; Kiziltay, A.; Hasirci, V.; Hasirci, N. PCL and PCL-Based Materials in Biomedical Applications. *J. Biomater. Sci., Polym. Ed.* **2018**, *29*, 863−893.
(24) Placone, J. K.; Engler, A. J. Recent Advances in Extrusion Based 3D printing for Biomedical Applications. *Adv. Healthcare Mater.* **2018**, *7*, 1701161.
(25) Nyberg, E.; Rindone, A.; Dorafshar, A.; Grayson, W. L. Comparison of 3D-printed Poly-e-caprolactone Scaffolds Functionalized with Tricalcium Phosphate; Hydroxyapatite; Bio-Oss; or Decellularized Bone Matrix. *Tissue Eng., Part A* **2017**, *23*, 503−514.
(26) Gómez-Lizárraga, K. K.; Flores-Morales, C.; Del Prado-Audelo, M. L.; Álvarez-Pérez, M. A.; Piña-Barba, M. C.; Escobedo, C. Polycaprolactone- and Polycaprolactone/Ceramic-based 3D-Bioplotted Porous Scaffolds for Bone Regeneration: A Comparative Study. *Mater. Sci. Eng., C* **2017**, *79*, 326−335.
(27) Neufurth, M.; Wang, X.; Wang, S.; Steffen, R.; Ackermann, M.; Haep, N. D.; Schröder, H. C.; Müller, W. E. G. 3D Printing of Hybrid Biomaterials for Bone Tissue Engineering: Calcium-Polyphosphate Micoparticles Encapsulated by Polycaprolactone. *Acta Biomater.* **2017**, *64*, 377−388.
(28) Kokubo, T.; Kushitani, H.; Ohtsuki, C.; Sakka, S. Chemical Reaction of Bioactive Glass and Glass-Ceramic with a Simulated Body Fluid. *J. Mater. Sci.: Mater. Electron.* **1992**, *3*, 79−83.
(29) Hamilton, R. D.; Leach, L. Isolation and Properties of An In Vitro Human Outer Blood-Retinal Barrier Model. *Methods Mol. Biol.* **2011**, *686*, 401−416.
(30) Lindroos, B.; Boucher, S.; Chase, L.; Kuokkanen, H.; Huhtala, H.; Haataja, R.; Vemuri, M.; Suuronen, R.; Miettinen, S. Serum-Free; Xeno-Free Culture Media Maintain the Proliferation Rate and Multipotentiality of Adipose Stem Cells In Vitro. *Cytotherapy* **2009**, *11*, 958−972.
(31) Tirkkonen, L.; Haimi, S.; Huttunen, S.; Wolff, J.; Pirhonen, E.; Sandor, G. K. Osteogenic Medium is Superior to Growth Factors in Differentiation of Human Adipose Stem Cells towards Bone-Forming Cells in 3D Culture. *Eur. Cell. Mater.* **2013**, *25*, 144−158.
(32) Ojansivu, M.; Vanhatupa, S.; Björkvik, L.; Häkkänen, H.; Kellomäki, M.; Autio, R.; Ihalainen, J. A.; Hupa, L.; Miettinen, S. Bioactive Glass Ions as Strong Enhancers of Osteogenic Differentiation in Human Adipose Stem Cells. *Acta Biomater.* **2015**, *21*, 190−203.
(33) Pfaffl, M. W. A New Mathematical Model for Relative Quantification in Real-Time RT-PCR. *Nucleic Acids Res.* **2001**, *29*, No. 45e.
(34) Hutmacher, D. W.; Schantz, T.; Zein, I.; Ng, K. W.; Teoh, S. H.; Tan, K. C. Mechanical Properties and Cell Cultural Response of Polycaprolactone Scaffolds Designed and Fabricated via Fused Deposition Modeling. *J. Biomed. Mater. Res.* **2001**, *55*, 203−216.
(35) Morouço, P.; Biscaia, S.; Viana, T.; Franco, M.; Malça, C.; Mateus, A.; Moura, C.; Ferreira, F. C.; Mitchell, G.; Alves, N. M. Fabrication of Poly(ε-caprolactone) Scaffolds Reinforced with Cellulose Nanofibers; with and without the Addition of Hydroxyapatite Nanoparticles. *BioMed Res. Int.* **2016**, *2016*, 1596157.
(36) Hannink, G.; Arts, J. J. C. Bioresorbability; Porosity and Mechanical Strength of Bone Substitutes: What is Optimal for Bone Regeneration? *Injury* **2011**, *42*, S22−S25.
(37) Loh, Q. L.; Choong, C. Three-Dimensional Scaffolds for Tissue Engineering Applications: Role of Porosity and Pore Size. *Tissue Eng., Part B* **2013**, *19*, 485−502.
(38) Murphy, C. M.; O'Brien, F. J. Understanding the Effect of Mean Pore Size on Cell Activity in Collagen-Glycosaminoglycan Scaffolds. *Cell Adh. Migr.* **2010**, *4*, 377−381.
(39) Bracaglia, L. G.; Smith, B. T.; Watson, E.; Arumugasaamy, N.; Mikos, A. G.; Fisher, J. P. 3D printing for the Design and Fabrication of Polymer-Based Gradient. *Acta Biomater.* **2017**, *56*, 3−13.
(40) Rai, V.; Dilisio, M. F.; Dietz, N. E.; Agrawal, D. K. Recent Strategies in Cartilage Repair: A Systemic Review. *J. Biomed. Mater. Res., Part A* **2017**, *105A*, 2343−2354.
(41) Keaveny, T. M.; Morgan, E. F.; Yeh, O. C. Bone Mechanics. In *Standard Handbook of Biomedical Engineering and Design*; Kutz, M., Ed.; McGraw-Hill: New York, 2004; pp 8.1−8.23, ISBN:9780071356374.
(42) Hench, L. L. Genetic Design of Bioactive Glass. *J. Eur. Ceram. Soc.* **2009**, *29*, 1257−1265.
(43) Lam, C. X. F.; Teoh, S. H.; Hutmacher, D. W. Comparison of the Degradation of Polycaprolactone and Polycaprolactone−(β-Tricalcium Phosphate) Scaffolds in Alkaline Medium. *Polym. Int.* **2007**, *56*, 718−728.
(44) Qazi, T. H.; Hafeez, S.; Schmidt, J.; Duda, G. N.; Boccaccini, A. R.; Lippens, E. Comparison of the Effects of 45S5 and 1393 Bioactive Glass Microparticles on hMSC behavior. *J. Biomed. Mater. Res., Part A* **2017**, *105A*, 2772−2782.
(45) Yeh, C.-H.; Chen, Y.-W.; Shie, M.-Y.; Fang, H.-Y. Poly(Dopamine)-Assisted Immobilization of Xu Duan on Printed Poly(Lactic Acid) Scaffolds to Up-Regulate Osteogenic and Angiogenic Markers of Bone Marrow Stem Cells. *Materials* **2015**, *8*, 4299−4315.
(46) Rodríguez, J. P.; Ríos, S.; González, M. Modulation of the Proliferation and Differentiation of Human Mesenchymal Stem Cells by Copper. *J. Cell. Biochem.* **2002**, *85*, 92−100.
(47) Rath, S. N.; Brandl, A.; Hiller, D.; Hoppe, A.; Gbureck, U.; Horch, R. E.; Boccaccini, A. R.; Kneser, U. Bioactive Copper-Doped Glass Scaffolds Can Stimulate Endothelial Cells in Co-Culture in Combination with Mesenchymal Stem Cells. *PLoS One* **2014**, *9*, No. e113319.
(48) Komori, T.; Groner, Y.; Ito, Y.; Liu, P.; Neil, J. C.; Speck, N. A.; van Wijnen, A. Roles of Runx2 in Skeletal Development. *Adv. Exp. Med. Biol.* **2017**, *962*, 962.
(49) Lian, J. B.; Stein, G. S. Development of the Osteoblast Phenotype: Molecular Mechanisms Mediating Osteoblast Growth and Differentiation. *Iowa Orthop. J.* **1995**, *15*, 118−140 PMCID: PMC2329080 .
(50) Lian, J. B.; Stein, G. S.; van Wijnen, A. J.; Stein, J. L.; Hassan, M. Q.; Gaur, T.; Zhang, Y. MicroRNA Control of Bone Formation and Homeostasis. *Nat. Rev. Endocrinol.* **2012**, *8* (4), 212−227.
(51) Li, S.; Wang, M.; Chen, X.; Li, S.; Li-Ling, J.; Xie, H. Inhibition of Osteogenic Differentiation of Mesenchymal Stem Cells by Copper Supplementation. *Cell Proliferation* **2014**, *47*, 81−90.
(52) Bührer, G.; Rottensteiner, U.; Hoppe, A.; Detsch, R.; Dafinova, D.; Fey, T.; Greil, P.; Weis, C.; Beier, J. P.; Boccacini, A. R.; Horch, R. E.; Arkudas, A. Evaluation of in vivo angiogenetic effects of copper doped bioactive glass scaffolds in the AV loop model. *Biomed. Glasses* **2016**, *2*, 111−117.

DOI: 10.1021/acsbiomaterials.9b00105
ACS Biomater. Sci. Eng. 2019, 5, 4496−4510